© 2018. Published by The Company of Biologists Ltd | Development (2018) 145, dev172650. doi:10.1242/dev.172650

CORRECTION

Correction: An essential role of CBL and CBL-B ubiquitin ligases in mammary stem cell maintenance (doi: 10.1242/dev.138164)

Bhopal Mohapatra, Neha Zutshi, Wei An, Benjamin Goetz, Priyanka Arya, Timothy A. Bielecki, Insha Mushtaq, Matthew D. Storck, Jane L. Meza, Vimla Band and Hamid Band

There was an error in Development (2018) **144**, dev138164 (doi: 10.1242/dev.138164).

One of the author names was spelled incorrectly. The online version has been corrected.

The authors apologise to readers for this mistake.

© 2017. Published by The Company of Biologists Ltd | Development (2017) 144, 1072-1086 doi:10.1242/dev.138164

STEM CELLS AND REGENERATION

RESEARCH ARTICLE

An essential role of CBL and CBL-B ubiquitin ligases in mammary stem cell maintenance

Bhopal Mohapatra[1,2,*], Neha Zutshi[1,3,*], Wei An[1,4], Benjamin Goetz[1], Priyanka Arya[1,4], Timothy A. Bielecki[1], Insha Mushtaq[1,3], Matthew D. Storck[1], Jane L. Meza[5], Vimla Band[1,4,6] and Hamid Band[1,2,3,4,6,‡]

ABSTRACT

The ubiquitin ligases CBL and CBL-B are negative regulators of tyrosine kinase signaling with established roles in the immune system. However, their physiological roles in epithelial tissues are unknown. Here, we used MMTV-Cre-mediated *Cbl* gene deletion on a *Cbl-b* null background, as well as a tamoxifen-inducible mammary stem cell (MaSC)-specific *Cbl* and *Cbl-b* double knockout (*Cbl*/*Cbl-b* DKO) using Lgr5-EGFP-IRES-CreERT2, to demonstrate a mammary epithelial cell-autonomous requirement of CBL and CBL-B in the maintenance of MaSCs. Using a newly engineered tamoxifen-inducible *Cbl* and *Cbl-b* deletion model with a dual fluorescent reporter (*Cbl*$^{flox/flox}$*; Cbl-b*$^{flox/flox}$*; Rosa26-CreERT; mT*/*mG*), we show that *Cbl*/*Cbl-b* DKO in mammary organoids leads to hyperactivation of AKT-mTOR signaling with depletion of MaSCs. Chemical inhibition of AKT or mTOR rescued MaSCs from *Cbl*/*Cbl-b* DKO-induced depletion. Our studies reveal a novel, cell-autonomous requirement of CBL and CBL-B in epithelial stem cell maintenance during organ development and remodeling through modulation of mTOR signaling.

KEY WORDS: Mammary gland development, Lgr5, Mammary stem cells, Basal cells, Luminal cells, mTOR signaling, CBLB, Casitas B-lineage lymphoma, Mouse

INTRODUCTION

Postnatal organ development and maintenance require organ-resident stem cells. While mechanisms of hematopoietic stem cell (HSC) maintenance are well understood, those that maintain epithelial stem cells have only recently become a focus of investigation. This is in part due to the rapid turnover of many epithelia and an emerging interest in the stem cell-like hierarchy of cancers, the clear majority of which originate in epithelial tissues. The mammary gland (MG) provides an excellent model to examine the mechanisms of adult epithelial stem cell maintenance, since a large part of ductal growth and branching takes place during pubertal development (Robinson et al., 2001; Gjorevski and Nelson, 2011).

[1]Eppley Institute for Research in Cancer and Allied Diseases, University of Nebraska Medical Center, Omaha, NE 68198, USA. [2]Department of Biochemistry & Molecular Biology, University of Nebraska Medical Center, Omaha, NE 68198, USA. [3]Department of Pathology & Microbiology, University of Nebraska Medical Center, Omaha, NE 68198, USA. [4]Department of Genetics, Cell Biology & Anatomy, College of Medicine, University of Nebraska Medical Center, Omaha, NE 68198, USA. [5]Department of Biostatistics, College of Public Health, University of Nebraska Medical Center, Omaha, NE 68198, USA. [6]Fred & Pamela Buffet Cancer Center, University of Nebraska Medical Center, Omaha, NE 68198, USA.
*These authors contributed equally to this work

‡Author for correspondence (hband@unmc.edu)

H.B., 0000-0002-4996-9002

Received 5 April 2016; Accepted 29 December 2016

Recently developed approaches to isolate and propagate mammary stem cells (MaSCs) *in vitro*, and to examine their self-renewal, differentiation and organ-regenerating abilities, make them excellent models to investigate mechanisms of epithelial stem cell homeostasis (Stingl et al., 2006a,b; Visvader, 2009). A better understanding of these mechanisms is important given the similarities of normal and cancer stem cell hierarchies and gene expression (Beck and Blanpain, 2013; Nguyen et al., 2012), as well as the prognostic significance of MaSC transcriptional signatures in breast cancer patients (Pece et al., 2010; Siegel and Muller, 2010; Soady et al., 2015).

Signaling pathways that regulate MG development also regulate MaSCs. For example, the Wnt signaling pathway regulates mammary development as well as MaSC self-renewal (van Amerongen et al., 2012). Wnt ligands help propagate MaSCs *in vitro* (Kessenbrock et al., 2013; Wang et al., 2013; Zeng and Nusse, 2010) and partly mediate the hormonal regulation of MaSCs (Cai et al., 2014). The Wnt pathway target gene *Lgr5*, which marks epithelial stem cells in the intestine, skin and other tissues (Barker et al., 2007, 2013), was recently shown to mark MaSCs (Plaks et al., 2013; Rios et al., 2014). Lgr5^{+} MaSCs can regenerate a MG upon transplantation (Plaks et al., 2013). Recently, Lgr5 was reported to be among the top 5% of 329 genes that are highly expressed in the MaSCs present among basal cells, as compared with other mammary epithelial cell (MEC) populations (Soady et al., 2015).

Receptor tyrosine kinases (RTKs), including members of the ErbB family, c-MET, RON, IGFR1/2, ephrin A2, among others, regulate MG development and MaSC maintenance (Gjorevski and Nelson, 2011; Hynes and Watson, 2010). FGFR2, for example, is crucial for MaSC maintenance (Pond et al., 2013) and RTK ligands are required for *in vitro* culture of MaSCs (Dontu et al., 2003; Guo et al., 2012). Dysregulation of precise signaling from RTKs and other receptors often leads to oncogenesis (Hynes and Watson, 2010; Korkaya et al., 2008).

Members of the CBL family (CBL, CBL-B and CBL-C in mammals) of ubiquitin ligases serve as negative regulators of protein tyrosine kinases (PTKs), including RTKs and non-receptor PTKs (Mohapatra et al., 2013). In contrast to substantial evidence supporting key physiological roles of CBL proteins (CBL/CBL-B) in hematopoietic and immune systems (An et al., 2015; Duan et al., 2004; Naramura et al., 2010; Thien and Langdon, 2005), their roles in epithelial tissues are essentially unknown. *Cbl-c* (also known as *Cblc*) mRNA is primarily expressed in epithelia, but a protein product has not been clearly demonstrated in such epithelia, and germline *Cbl-c* deletion is without an overt phenotype (Griffiths et al., 2003). A mammary epithelium-intrinsic role of CBL family proteins remains unknown. Transcriptome data show that CBL and CBL-B are expressed in the mammary epithelium, with CBL-B expression enriched in MaSCs (Lim et al., 2010). The embryonic lethality of germline *Cbl* and *Cbl-b* (also known as *Cblb*) double

Development (2017) 144, 1072-1086 doi:10.1242/dev.138164

knockout (*Cbl*/*Cbl-b* DKO) in mice (Naramura et al., 2002), the exaggeration of immune phenotypes of *Cbl-b* deficiency by conditional *Cbl* deletion in immune cells (Kitaura et al., 2007; Naramura et al., 2002), a myeloproliferative disorder (MPD) upon *Cbl*/*Cbl-b* DKO in HSCs (An et al., 2015; Naramura et al., 2010), and the apparent lack of mammary epithelial-intrinsic and other epithelial phenotypes in $Cbl^{-/-}$ or $Cbl\text{-}b^{-/-}$ mice strongly suggest redundant functions of CBL and CBL-B in epithelia.

To investigate the epithelial cell-intrinsic roles of CBL and CBL-B, we used a conditional DKO model in which floxed *Cbl* was selectively deleted in the mammary epithelium on a germline $Cbl\text{-}b^{-/-}$ background using MMTV-Cre (Wagner et al., 1997). Since concomitant DKO in a small fraction of HSCs in this model leads to a MPD (An et al., 2015; Naramura et al., 2010), we characterized the MG development prior to significant MPD and by using a transplant approach. These analyses revealed a redundant but essential epithelium-intrinsic requirement for CBL and CBL-B in pubertal MG development. *Cbl/Cbl-b* DKO mammary epithelium exhibited shrinkage of the MaSC-containing basal compartment, which led us to develop a novel MaSC-specific *Cbl/Cbl-b* DKO model in which floxed *Cbl* is inducibly deleted only in $Lgr5^{+}$ MaSCs. We also generated a novel mouse model in which floxed *Cbl* and *Cbl-b* can be inducibly deleted in isolated basal MECs upon tamoxifen treatment (Goetz et al., 2016). Complementary evidence from these genetic models establishes that CBL and CBL-B are redundantly required to maintain MaSCs, apparently by controlling the level of AKT-mTOR signaling.

RESULTS

MMTV-Cre-mediated *Cbl* deletion on a *Cbl-b* null background (conditional DKO) leads to impaired mouse MG development

Real-time qPCR analyses of FACS-purified luminal and basal cell fractions of the mouse MG confirmed that all three CBL family genes are expressed in epithelial compartments (Fig. S1A). Since an endogenous CBL-C protein remains to be demonstrated (Mohapatra et al., 2013), while strong evidence supports redundant but crucial roles of CBL and CBL-B (Mohapatra et al., 2013; Naramura et al., 2002), we investigated the impact of mammary epithelial-intrinsic *Cbl* and *Cbl-b* DKO using *Cbl-b* null mice with MMTV-Cre-induced mammary epithelial deletion of floxed *Cbl* and expression of *lacZ* reporter (Naramura et al., 2010). The Cre^{+} $Cbl^{f/+}$; $Cbl\text{-}b^{+/-}$ littermates served as Cre controls. X-gal staining of MG whole-mounts at 5-6 weeks of age indicated efficient Cre-mediated recombination in both control and DKO mice (Fig. S1B). Concurrent nuclear Fast Red and X-gal staining confirmed recombination in both luminal and basal compartments (Fig. S1C). Separately, the expression of a GFP reporter confirmed the MMTV-Cre-mediated gene deletion in the DKO and Cre control mice (Fig. S1D).

Since MMTV-Cre-induced DKO leads to MPD by 10 weeks of age, we analyzed the postnatal MG growth in 5-, 7- and 9-week-old virgin females. Compared with littermate controls, the DKO mice exhibited significantly retarded mammary ductal outgrowths (Fig. 1A), with significant reduction in the number of branch points, ductal length and fat pad filling (Fig. 1B-D). Western blotting (WB) confirmed the CBL deletion and the lack of CBL-B expression in DKO MGs (Fig. 1E), and immunohistochemical (IHC) staining revealed this to be in the mammary epithelium (Fig. 1F). *Cbl-b* KO mice show a compensatory increase in CBL expression in several tissues, including MG (Fig. 1E).

Hematoxylin and Eosin (H&E) staining of sections revealed sparser ducts in the MGs of 6-week-old DKO mice, but the overall basal and luminal layers were intact (Fig. S2A), a conclusion confirmed by immunofluorescence staining for basal [keratin 5 (K5)] and luminal [keratin 8 (K8)] cytokeratins (Fig. S2B).

The smaller size of DKO MGs could reflect reduced proliferation, increased apoptosis, or both, as their balance is important in mammary morphogenesis (Humphreys et al., 1996; McCaffrey and Macara, 2009). Ki67 staining showed reduced proliferation in DKO mammary ducts but not in terminal end buds (TEBs), compared with controls (Fig. S2C-F). Cleaved caspase-3 staining revealed a comparable level of apoptosis in the TEBs of control and DKO mice (Fig. S2G).

Although the analyses above were performed prior to overt MPD development, we used a transplantation approach (Deome et al., 1959; Stingl et al., 2006a,b) to rule out the possibility that subclinical MPD might have impaired MG development. Contralateral transplantation of control and DKO mammary tissue was performed in NSG hosts. Carmine alum and X-gal staining of MG whole-mounts 10 weeks post-transplant revealed significantly less fat pad filling and reduced branching in DKO transplants (Fig. S3A,B). Compared with the extensive growth and alveolar differentiation of control transplants during pregnancy, DKO transplants were dramatically smaller with less fat pad filling and reduced ductal elongation, although the alveolar differentiation appeared intact (Fig. S3B).

Next, to address whether the DKO phenotype was MEC-autonomous, FACS-sorted lineage-negative (Lin^{-}; epithelial and stromal cells) or $Lin^{-}/EpCAM^{+}$ (epithelial cells only) MECs from 6-week-old *Cbl/Cbl-b* DKO versus control donors were transplanted in NSG mice. Whereas all the control Lin^{-} or $Lin^{-}/EpCAM^{+}$ MEC transplants led to mammary outgrowths, none of the DKO transplants showed any outgrowths (Fig. S3C,D). Together, our results conclusively demonstrate that deletion of *Cbl* and *Cbl-b* in MECs leads to a cell-autonomous impairment of MG growth and branching.

Cbl/*Cbl-b* DKO shrinks the MaSC-containing basal MEC population

Impaired MG development in *Cbl/Cbl-b* DKO mice and their inability to regenerate the mammary epithelium upon transplant suggested potential impairment of DKO MaSCs. We therefore analyzed dissociated MECs from 6- or 8-week-old control or DKO mice by FACS, with staining for CD29 (ITGB1), CD24 and EpCAM, which separate MECs into basal ($CD29^{hi}$ $CD24^{+}$ or $EpCAM^{low}$ $CD29^{hi}$) and luminal ($CD29^{low}$ $CD24^{+}$ or $EpCAM^{hi}$ $CD29^{low}$) populations (Shehata et al., 2012; Smalley et al., 2012). The former includes MaSCs and mature myoepithelial cells, whereas the latter includes luminal progenitors and mature luminal cells (Shackleton et al., 2006; Stingl et al., 2006a,b). Although we used both CD24/CD29 and EpCAM/CD29 combinations, better separation of subsets was seen in FACS plots with EpCAM/CD29 combination (Fig. S4A,B). This analysis revealed that *Cbl/Cbl-b* DKO MGs yielded significantly fewer $Lin^{-}/EpCAM^{+}$ MECs in total, consistent with reduced MG size in these mice (Fig. S5A,B). Notably, the basal cell percentage was significantly lower, both at 6 and 8 weeks, with a corresponding increase in the proportion of luminal cells (Fig. 2A-D). However, the absolute number of luminal cells was reduced in DKO MGs (Fig. S5B,C). Given the overall reduction in the number of MECs in DKO mice (Fig. S5B,D), the smaller size of their basal MEC compartment suggested a particularly severe reduction in all or some of the cell types that comprise this compartment (Yamaji et al., 2009).

Development (2017) 144, 1072-1086 doi:10.1242/dev.138164

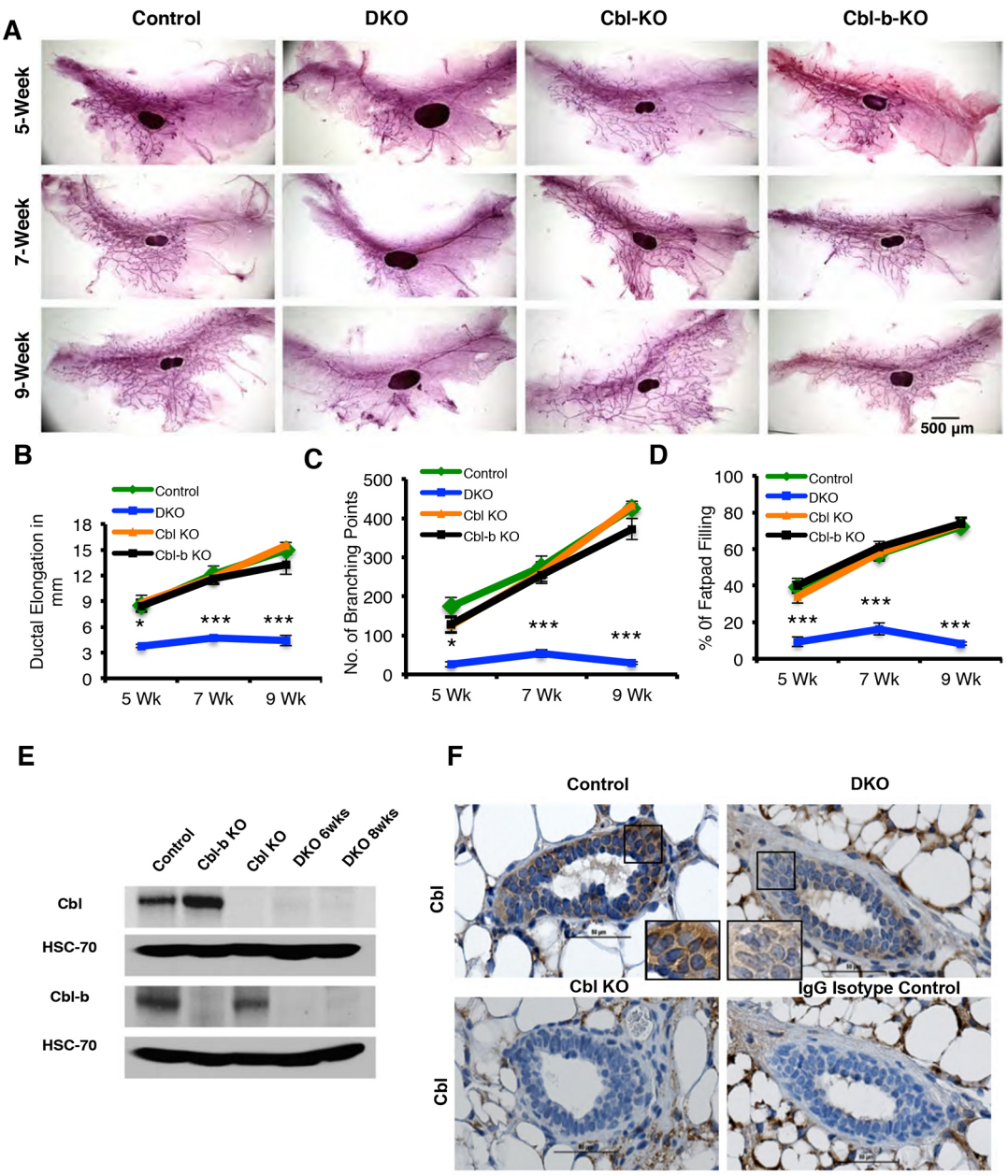

Fig. 1. Impaired mammary gland (MG) development in *Cbl*/*Cbl-b* DKO mice. (A) Carmine alum-stained whole-mounts of *Cbl*/*Cbl-b* DKO, *Cbl* KO and *Cbl-b* KO virgin female mice at 5, 7 and 9 weeks of age. (B-D) Images as in A were analyzed to quantify differences in ductal length (B), number of branch points (C) and percentage of fat pad filling (D). Data represent mean±s.e.m. of four animals per group. *$P \leq 0.05$, ***$P \leq 0.001$ (Student's *t*-test). (E) Whole MG lysates from 6-week-old control, *Cbl-b* KO or *Cbl* KO, and 6- or 8-week-old *Cbl*/*Cbl-b* DKO mice were blotted with antibodies against CBL, CBL-B or HSC70 (HSPA8) to reveal deletion of CBL and CBL-B according to genotype. (F) IHC of MG sections from 6-week-old control, *Cbl*/*Cbl-b* DKO and *Cbl* KO mice with anti-CBL monoclonal antibody was performed using avidin-biotin amplification. CBL staining (brown) is seen in epithelial cells lining the ducts in control but not in DKO MG. Inset shows magnified images of brown staining seen in control not in DKO.

The purity of FACS-sorted basal or luminal cells was verified by K5 or K8 expression, respectively (Lim et al., 2010) (Fig. S6A,B). qPCR analysis of purified cell populations showed that *Cbl* and *Cbl-b* were expressed in control MECs but undetectable (*Cbl* signal <0.02% and *Cbl-b* signal <0.003% of wild type) in DKO MECs (Fig. S6C). *Cbl-b* expression was enriched in the basal compartment of control mice, consistent with previous microarray data (Lim et al., 2010). Recent studies have shown that the basal $K5^+$ postnatal mouse MEC population contains bi-potent MaSCs, whereas the luminal $K8^+$ population includes the luminal lineage-restricted progenitors (Rios et al., 2014). Quantification of mRNA levels in FACS-sorted populations by qPCR revealed reduced *K5* levels in the basal compartment and increased *K8* levels in the luminal compartment of DKO versus control mice (Fig. S6D,E).

We confirmed these findings using 6-week-old GFP reporter-bearing control and DKO mice, in which the GFP^+ MECs represent the progeny of MMTV-Cre-expressing cells. These analyses also demonstrated a reduction in the basal cell population and a relative increase in the luminal fraction in DKO mice (Fig. 2E,F).

CD61 (ITGB3) and CD29 co-staining separates virgin MG MECs into populations that harbor MaSCs ($CD29^{hi}$ $CD61^-$), luminal progenitors ($CD29^{low}$ $CD61^+$), mature luminal cells

Development (2017) 144, 1072-1086 doi:10.1242/dev.138164

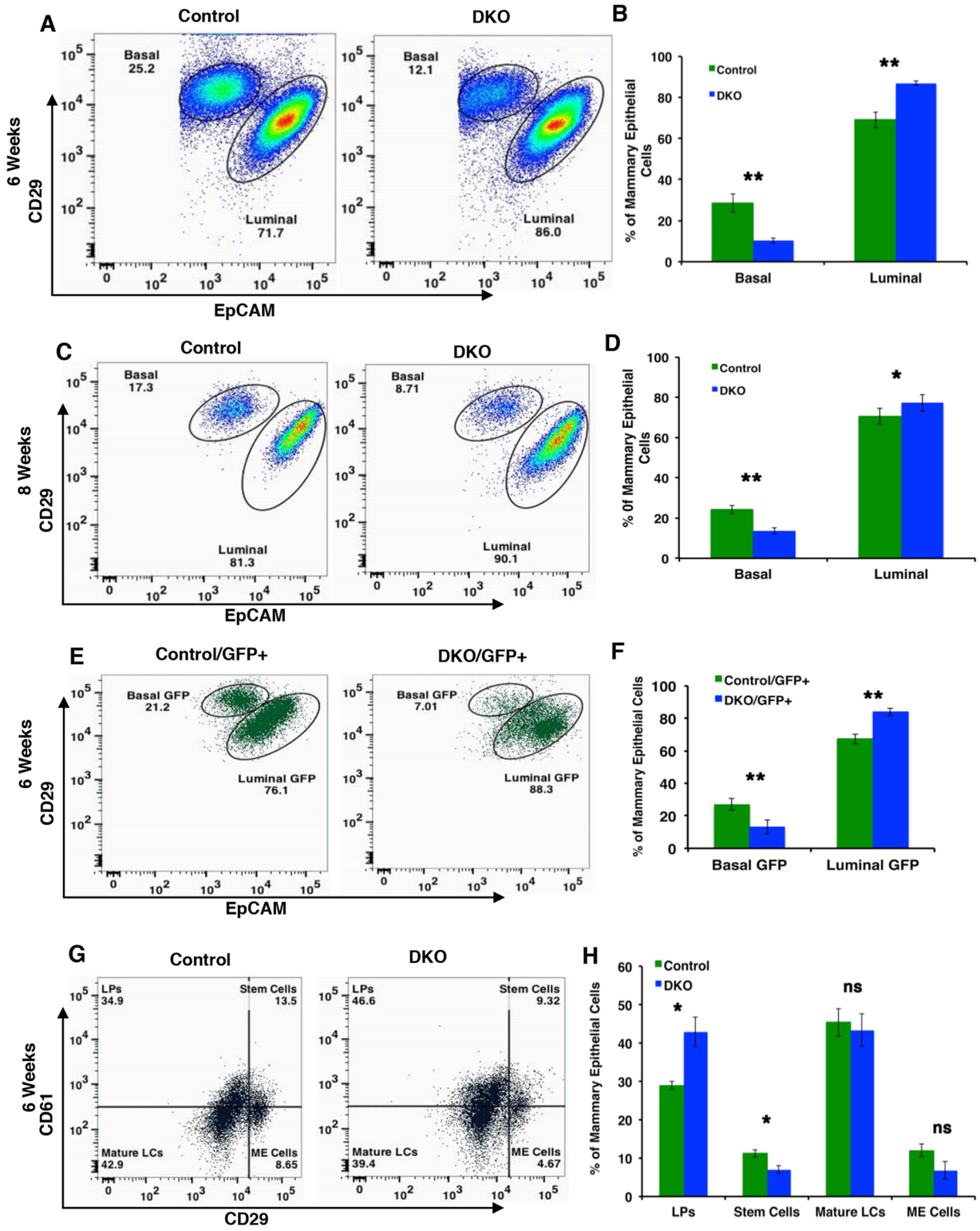

Fig. 2. Isolated MMTV-Cre-induced *Cbl*/*Cbl-b* DKO mammary epithelial cells (MECs) show a reduction in the proportion of basal cells with a relative increase in the proportion of luminal cells. (A,C) Representative pseudocolored FACS plots, gating on basal ($CD29^{hi}$ $EpCAM^{low}$) and luminal ($CD29^{low}$ $EpCAM^{hi}$) populations, show a smaller basal and a larger luminal subset in DKO versus control mice. (B,D) Quantitation of the relative percentages at 6 weeks (B, n=9) and 8 weeks (D, n=5) of age. (E) GFP^+ basal and luminal cell subsets of control versus *Cbl*/*Cbl-b* DKO mice bearing a GFP reporter, indicating a reduction in the basal population and increase in the luminal population in DKO compared with control. (F) Quantitation of the percentage of basal and luminal GFP^+ cells in *Cbl*/*Cbl-b* DKO compared with control mice (n=4) (as in E). (G) FACS dot plots showing mammary stem cell (MaSC), luminal progenitor (LP), mature luminal cell (LC) and myoepithelial cell (ME) populations. *Cbl*/*Cbl-b* DKO mice show a reduction in the proportions of stem cells, LCs and MEs, and an increase in the proportion of LPs compared with control mice (numbers within quadrants indicate percentage of total). (H) Quantitation of the relative percentages of stem cell, LP, LC and ME populations (as in G) in control versus DKO mice (n=6). Data are mean±s.e.m. ns, $P \geq 0.05$; *$P \leq 0.05$, **$P \leq 0.01$ (Student's t-test). Note that differences in the percentage of cells within the stem cell and LP compartments are significant.

Development (2017) 144, 1072-1086 doi:10.1242/dev.138164

(CD29^{low} CD61^{-}) and mature myoepithelial cells (CD29^{hi} CD61^{+}) (Carr et al., 2012; Shackleton et al., 2006; Stingl et al., 2006a,b). CD29 and CD61 co-staining and FACS analysis of MECs from 6-week-old control and DKO mice revealed that DKO MECs exhibited a significant increase in the proportion of luminal progenitors and a marked reduction of MaSCs, suggesting that *Cbl/Cbl-b* DKO promotes a shift of MaSCs towards luminal progenitors (Fig. 2G,H). However, we did not observe a proportionate increase in the mature luminal cell pool, suggesting that the DKO luminal progenitors are defective in their capacity to generate mature cells. The proportion of mature myoepithelial cells was comparable between control and DKO MECs.

Cbl/*Cbl-b* DKO basal MECs show reduced stem cell activity in organoid cultures *in vitro*

Organoid-forming ability in Matrigel reflects the stemness of MECs, with the MaSC-containing basal population yielding solid organoids and the luminal progenitor-containing luminal population yielding acini (Lim et al., 2009; Shackleton et al., 2006). Indeed, Matrigel culture of basal and luminal MEC populations, FACS sorted based on CD29/EpCAM (plus GFP reporter for DKO mice), showed that control MaSC-enriched basal cells form solid organoids with ∼6% efficiency, whereas luminal cells formed acini with hollow lumens at higher efficiencies (than 6%) but solid organoids only rarely (Fig. 3A). The ability of DKO basal MECs to form solid organoids was significantly reduced, whereas acini formation of DKO luminal cells was comparable to that of controls (Fig. 3B). Similar results were obtained after harvesting and replating the first passage organoids or acini for a second passage (Fig. 3C). qPCR at the end of passage 1 confirmed lack of *Cbl* and *Cbl-b* mRNA in organoids generated from DKO basal and luminal cells, excluding the possibility of organoids/acini having arisen from precursors in which floxed *Cbl* was not deleted (Fig. 3D). Altogether, these results further established that loss of CBL and CBL-B in the mammary epithelium impairs the ability of MaSCs to self-renew.

Lgr5-Cre-based conditional *Cbl*/*Cbl-b* DKO leads to shrinkage of the MaSC pool and their rapid transition into luminal progenitors

The Wnt target gene *Lgr5* was recently found to mark MaSCs within the basal MEC compartment (de Visser et al., 2012; Plaks et al., 2013); such cells were shown to be bi-potent and to regenerate the MG upon transplant (Plaks et al., 2013; Rios et al., 2014). We crossed the Lgr5-EGFP-IRES-CreERT2 mice with *Cbl$^{f/f}$; Cbl-b$^{-/-}$* mice to create mice for MaSC-selective and tamoxifen-inducible *Cbl/Cbl-b* DKO within the mammary epithelium. FACS analysis of MECs from parental Lgr5-GFP-Cre mice confirmed the presence of a small pool of Lgr5^{+} (*Lgr5*-driven GFP^{+}) cells nearly exclusively in the basal population (Plaks et al., 2013) (Fig. S7A,B). Importantly, within 5 days of initiating tamoxifen-induced *Cbl* deletion in the DKO model, the Lgr5^{+} cells underwent a significant shrinkage compared with control (*Cbl$^{f/+}$; Cbl-b$^{+/-}$*) mice (Fig. 4A,B). CD29/EpCAM-based assignment of GFP^{+} cells to basal and luminal compartments indicated that the proportion of Lgr5^{+} cells in the basal compartment decreased upon tamoxifen induction, whereas the proportion in the luminal compartment increased significantly (Fig. 4C), indicating a severe depletion of MaSCs, with a proportion of the DKO MaSCs transitioning into the luminal compartment. The tamoxifen-induced deletion of *Cbl* (and constitutive deletion of *Cbl-b*) in the sorted GFP^{+}, but not GFP^{-}, MEC fraction was confirmed by qPCR (Fig. 4D,E), clearly establishing the MaSC-selective DKO in the Lgr5-Cre-based model.

In vivo Cbl/*Cbl-b* DKO in MaSCs impairs their organoid-forming ability *in vitro*

To assess the impact of *in vivo* Lgr5-Cre-based *Cbl/Cbl-b* DKO in MaSCs on their stemness, GFP^{+} (Lgr5^{+}) MECs sorted from Lgr5-EGFP-Cre^{+} (MaSC control) or conditional DKO (MaSC DKO) mice 10 days post-tamoxifen were subjected to organoid-forming assays. Whereas Lgr5^{+} cells from MaSC control MGs formed solid organoids, Lgr5^{+} cells from tamoxifen-treated MaSC DKO mice produced significantly fewer and smaller organoids (Fig. 5A-C).

In vitro induction of *Cbl*/*Cbl-b* DKO in Lgr5^{+} MaSCs impairs their stemness

The number and size of organoids formed after 7 days of Matrigel culture from FACS-sorted GFP^{+} (Lgr5^{+}) MECs from uninduced MaSC control or conditional MaSC *Cbl/Cbl-b* DKO mice were comparable (Fig. 5D,G). Next, 4-hydroxytamoxifen (4-OH-T) was added on day 7 of culture and organoids were harvested after 96 h, replated, and examined after 8 days. Compared with uninduced cultures, 4-OH-T induction of Lgr5^{+} MECs significantly impaired the ability to form organoids upon replating (Fig. 5E,H). Further passaging confirmed these results (Fig. 5F,H). WB of harvested organoids verified CBL and CBL-B deletion (Fig. 5I,J). Organoid assays on Lgr5^{+} cells isolated from Lgr5-GFP-Cre^{+} conditional DKO mice and cultured in the presence of 4-OH-T also showed reduced organoid-forming ability, as compared culture in the absence of 4-OH-T, owing to *Cbl* deletion (as confirmed by qPCR; Fig. 6A-C).

Consistent with results in the MMTV-Cre-based DKO model, qPCR analysis showed that the levels of *K5* and *K14* were reduced in 4-OH-T-induced DKO organoids compared with non-induced controls, whereas the expression of *K8* increased (Fig. 6D-F). Immunofluorescence analyses showed an increase in the proportion of K8^{+} cells and a decrease in the proportion of K14^{+} cells in MaSC DKO organoids (Fig. 6G,H).

Depletion of MaSCs upon *Cbl* and *Cbl-b* deletion is mediated through hyperactivation of AKT-mTOR signaling

RTK signaling is crucial for MG development and the maintenance of MaSCs (Brisken et al., 2000; van Amerongen et al., 2012). PI3K-AKT-mTOR is a key signaling node downstream of activated RTK signaling (Sun and Bernards, 2014), and studies in cell models have shown that loss of *Cbl* or *Cbl-b* increases the levels of phosphorylated (p) AKT (An et al., 2015; Fang and Liu, 2001). Importantly, hyperactivation of AKT-mTOR signaling has been shown to promote differentiation and stem cell exhaustion in hematopoietic, neural and epidermal stem cell systems (Iglesias-Bartolome et al., 2012; Kalaitzidis et al., 2012; Magri et al., 2011). In view of reduced MG development and of MaSC depletion upon *Cbl/Cbl-b* DKO, we assessed whether AKT-mTOR signaling is hyperactivated in DKO MECs. As the number of cells available from the Lgr5-Cre-driven model was small, we used a fully tamoxifen-inducible *Cbl* and *Cbl-b* deletion model (Goetz et al., 2016) in which both *Cbl* and *Cbl-b* are floxed, and the *ROSA26* locus *CreERT* and dual fluorescent reporter (*mT/mG*) alleles allow verifiable 4-OH-T-inducible *in vitro Cbl* and *Cbl-b* deletion. The MaSC-containing basal cells from *Cbl$^{f/f}$; Cbl-b$^{f/f}$; CreERT; mT/mG* or *Cbl$^{f/f}$; Cbl-b$^{f/+}$; CreERT; mT/mG* mice were plated in organoid cultures and induced with 4-OH-T (Fig. 7A). Whereas uninduced organoids were uniformly RFP^{+}, 4-OH-T induction led to a switch

Development (2017) 144, 1072-1086 doi:10.1242/dev.138164

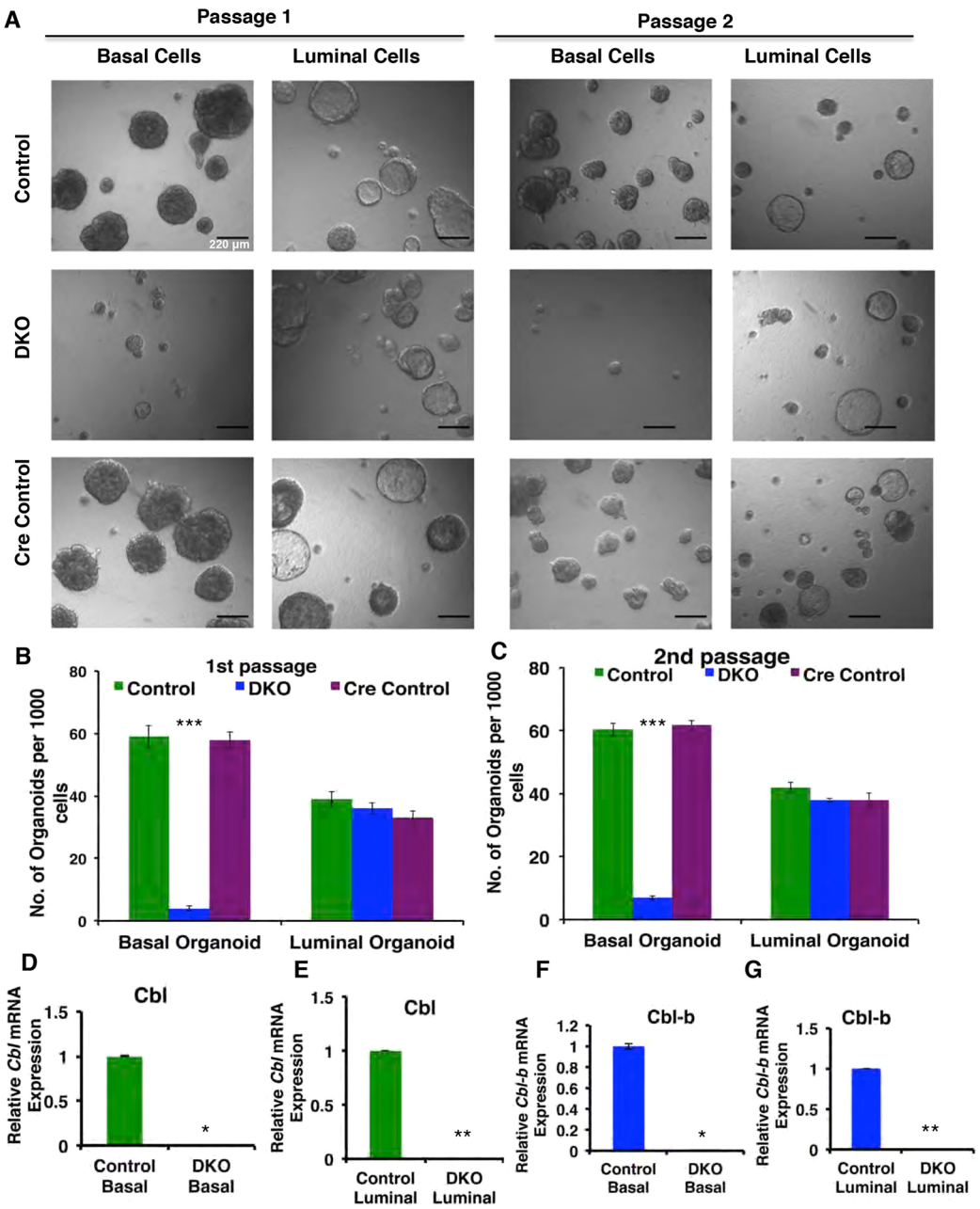

Fig. 3. Demonstration of impaired MaSC renewal in MMTV-Cre-driven *Cbl*/*Cbl-b* DKO basal MECs using the *in vitro* organoid-forming assay. (A) Basal and luminal MEC populations were isolated from MGs of control [*Cbl*$^{f/f}$; *Cbl-b*$^{+/-}$; *MMTV-Cre(0/0)*], Cre control [*Cbl*$^{f/+}$; *Cbl-b*$^{+/-}$; *MMTV-Cre(Tg/0)*] and *Cbl*/*Cbl-b* DKO [*Cbl*$^{f/f}$; *Cbl-b*$^{-/-}$; *MMTV-Cre(Tg/0)*] mice using FACS sorting with CD29 and EpCAM markers. Note that *MMTV-Cre(Tg/0)* refers to the Cre^{+} animal maintained as hemizygous transgene and *MMTV-Cre(0/0)* refers to Cre^{-}. Sorted cells were cultured in suspension and passaged a second time. Representative images of filled organoids formed by basal cells and acinar organoids formed by luminal cell populations are shown. Scale bar applies to all images in A. (B,C) The numbers of organoids greater than 100 µm in diameter were counted in three independent samples and expressed per 1000 seeded cells at first (B) and second (C) passage. (D-G) RNA isolated from organoids was used for qPCR to confirm the deletion of *Cbl* and lack of expression of *Cbl-b*. Data shown are mean±s.e.m. ns, $P \geq 0.05$; *$P \leq 0.05$, **$P \leq 0.01$, ***$P \leq 0.001$ (Student's *t*-test).

to GFP^{+} organoids, indicating robust CreERT-dependent gene deletion. WB verified CBL and CBL-B deletion, concurrent with upregulation of the levels of total and pEGFR, pAKT and pmTOR in 4-OH-T-induced DKO organoids as compared with uninduced organoids (Fig. 8A). Replating of uninduced versus induced *Cbl*$^{f/f}$; *Cbl-b*$^{f/f}$; *CreERT; mT/mG* organoids showed a substantial reduction in organoid growth upon *in vitro Cbl* and *Cbl-b* deletion (Fig. 7B,C), consistent with results of the MMTV-Cre and Lgr5-Cre models. PCR analysis of *Cbl* and *Cbl-b* expression showed significant reduction upon 4-OH-T induction (Fig. 7D,E). *Egfr* mRNA levels were not significantly upregulated upon 4-OH-T induction (Fig. 7F). Basal cell-derived organoids from *Cbl*$^{f/f}$; *Cbl-b*$^{f/+}$; *CreERT; mT/mG* mice showed only a slight reduction in organoid numbers upon induction (Fig. 7C, lower panels). qPCR analysis showed lower levels of *K14* and increased levels of *K8* in induced versus non-induced organoids, indicating differentiation towards luminal lineages (Fig. 7G,H). Luminal cells from *Cbl*$^{f/f}$; *Cbl-b*$^{f/f}$; *CreERT; mT/mG* mice yielded comparable numbers of organoids

Development (2017) 144, 1072-1086 doi:10.1242/dev.138164

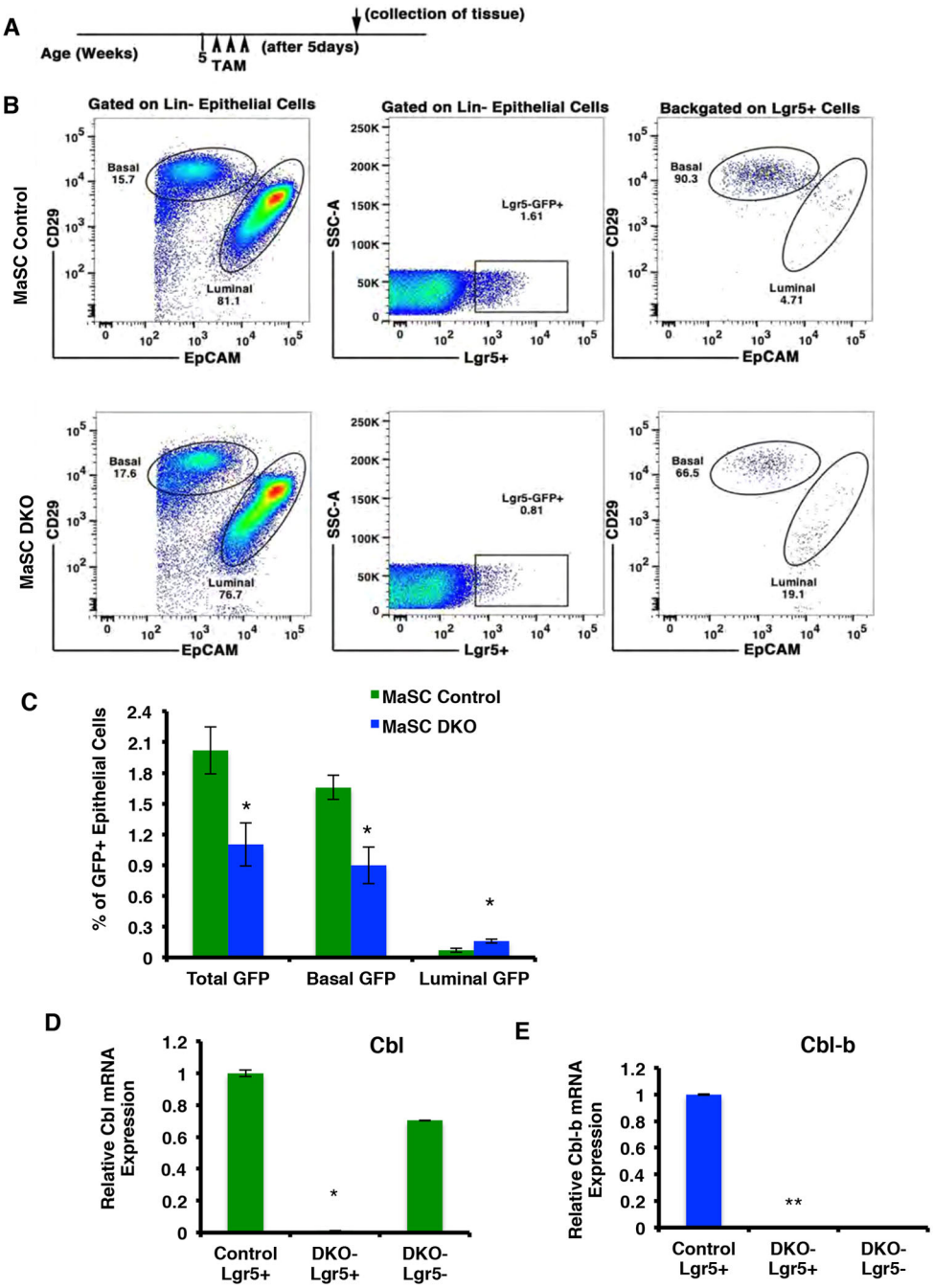

Fig. 4. Lgr5-CreERT-driven, tamoxifen-inducible MaSC-specific *Cbl*/*Cbl-b* DKO leads to shrinkage of the MaSC pool.
(A) Timeline of tamoxifen (TAM) induction and analysis. Five-week-old *Cbl*$^{fl/+}$; *Cbl-b*$^{+/-}$; *Lgr5-CreERT* (MaSC *Cbl* control) and *Cbl*$^{f/f}$; *Cbl-b*$^{-/-}$; *Lgr5-GFP-CreERT* (MaSC DKO mice) were given three daily injections of tamoxifen and analyzed 5 days after the last injection.
(B) Representative FACS plots of isolated Lin$^-$ MECs from MaSC control and MaSC DKO analyzed for GFP and CD29/EpCAM staining. Middle panel shows gating for Lgr5$^+$ (GFP$^+$) population and right panel represents compartmentalization of Lgr5$^+$ cells within the basal and luminal populations. Percentage of cells within each population is indicated.
(C) Percentage of total GFP$^+$ cells, and of GFP$^+$ cells within the basal and luminal populations, in MaSC DKO compared with control mice (n=6). (D,E) RNA isolated from FACS-sorted GFP$^+$ epithelial cells from MaSC control mice and GFP$^+$ and GFP$^-$ fractions of MaSC DKO Lin$^-$ cells was used for qPCR using primers specific to *Cbl* (D) and *Cbl-b* (E) to confirm Lgr5$^+$ cell-specific deletion of *Cbl* as well as lack of expression of *Cbl-b* in MaSC DKO mice. Data shown are mean±s.e.m. *P≤0.05, **P≤0.01 (Student's t-test).

with and without 4-OH-T induction (Fig. S8A), and WB analysis showed no changes in cyclin D1 (proliferation marker) expression (Fig. S8B). WB analyses also verified CBL and CBL-B depletion and an increase in pEGFR but without an increase in total EGFR, but relatively little impact on pAKT or pERK levels (Fig. S8B). Collectively, the results of inducible deletion of both *Cbl* and *Cbl-b* further support our conclusion that CBL and CBL-B are required for MaSC maintenance, and show that their deletion hyperactivates the AKT-mTOR signaling axis.

To assess whether AKT-mTOR hyperactivation might mediate the loss of MaSCs upon *Cbl* and *Cbl-b* deletion, we tested if specific AKT or mTOR inhibitors could rescue MaSCs from *Cbl/Cbl-b* DKO-induced depletion. The allosteric AKT inhibitor MK-2206 (Hirai et al., 2010; Yap et al., 2011) was added to preformed organoids generated from a *Cbl*$^{f/f}$; *Cbl-b*$^{f/f}$; *CreERT; mT/mG* basal cell population with or without concurrent 4-OH-T induction at 50 nM or 100 nM, based on IC_{50} values reported in other systems (Sangai et al., 2012). MK-2206 treatment markedly reduced AKT-pS473 levels, and partially reduced the levels of pmTOR (Fig. 8B). Direct mTOR inhibition with rapamycin, at 1 nM and 10 nM, led to reduction of pmTOR as well as AKT-pS473 (Fig. 8B), the latter an expected effect of prolonged rapamycin treatment causing inhibition of mTORC1 and mTORC2 complex activity (Ballou and Lin, 2008; Sarbassov et al., 2006; Weichhart et al., 2015). Replating of untreated versus inhibitor-treated organoids showed an inhibitor dose-dependent partial (AKT inhibitor) or complete (mTOR inhibitor) rescue of secondary organoid formation by *Cbl/Cbl-b* DKO cells as compared with the untreated control (Fig. 8C,D). These results support the conclusion that hyperactivation of mTOR signaling downstream of RTKs, in part

Development (2017) 144, 1072-1086 doi:10.1242/dev.138164

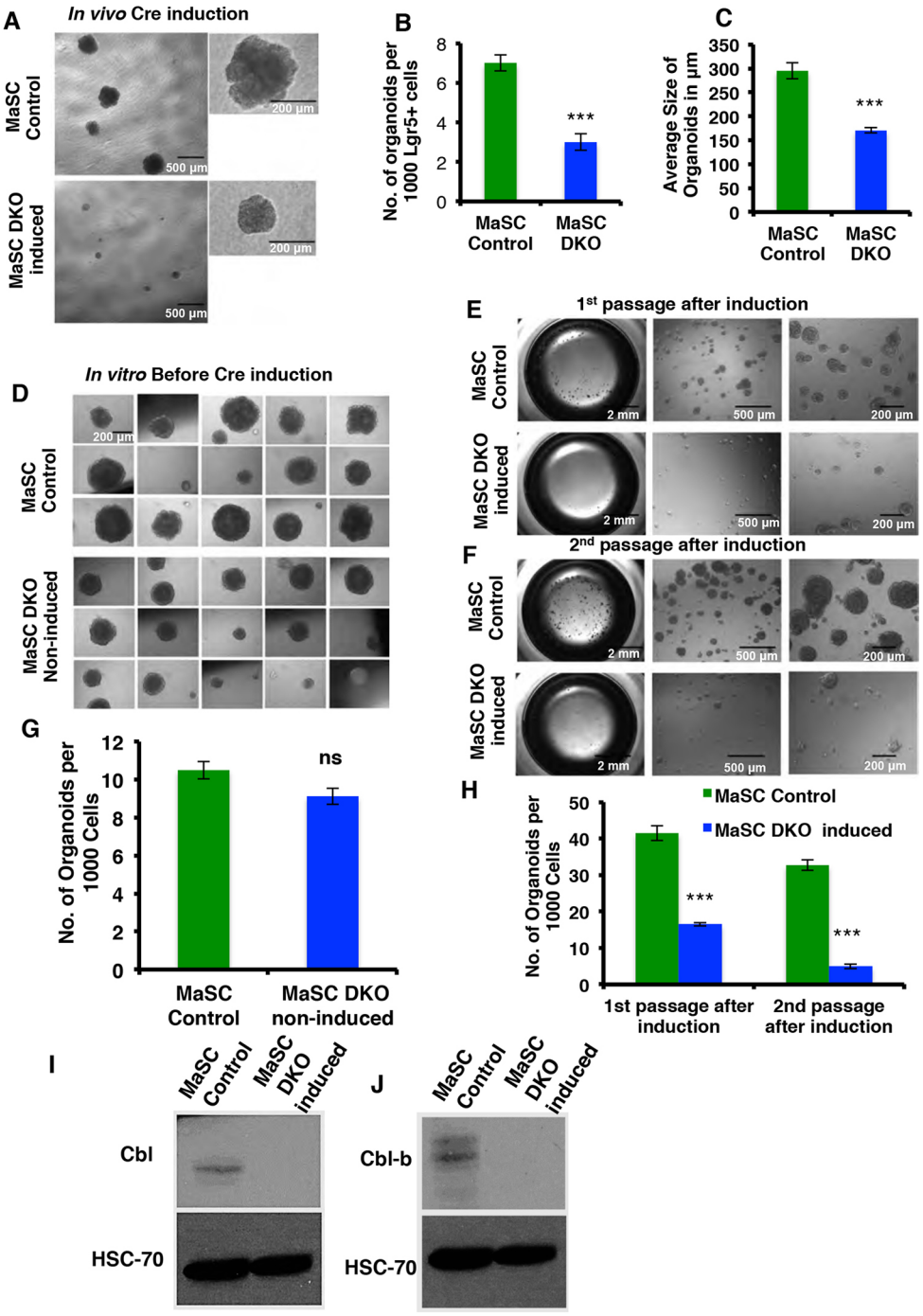

Fig. 5. *In vivo* or *in vitro* induction of Lgr5-CreERT to impart Lgr5$^+$ MaSC-selective *Cbl*/*Cbl-b* DKO leads to impaired MaSC self-renewal.
(A-C) MECs isolated 10 days post-induction of Lgr5-GFP-IRES-CreERT mice were assayed for organoid-forming ability. (A) Representative images of organoids cultured for 9 days in 100% Matrigel (insets are enlarged images). (B) Quantification of organoid numbers; n=3. (C) Quantification of organoid size (in µm); n=3. (D,G) FACS-sorted Lgr5$^+$ (GFP$^+$) MECs isolated from non-induced Lgr5-GFP-IRES-CreERT control and *Lgr5-GFP-CreERT; Cbl$^{f/f}$; Cbl-b$^{-/-}$* mice were cultured in 100% Matrigel for 10 days with 4-OH-T (400 nM final) added for the last 96 h. Comparable numbers of organoids were seen in MaSC control and DKO, as shown in representative pictures of organoids before 4-OH-T induction (D) and quantitation of results (G). The scale bar applies to all images in D. (E) The organoids were then dissociated and 2000 cells/well were cultured in 96-well ultra low-attachment plates in the presence of 5% Matrigel for 8 days, and imaged (first passage). (F) Likewise, secondary plating was performed. (H) Quantification of organoids after 4-OH-T induction of control and conditional DKO Lgr5$^+$ MaSCs at passage 1 and 2. (I,J) WB analysis of 4-OH-T induced control and DKO organoids at the end of the second passage for CBL, CBL-B and HSC70. Data (n=3) are shown as mean±s.e.m. ns, $P\geq0.05$; ***$P\leq0.001$ (Student's t-test).

due to hyperactivity of AKT, promotes the depletion of MaSCs in *Cbl/Cbl-b* DKO mammary epithelium.

DISCUSSION

CBL family ubiquitin ligases target active pools of PTKs for ubiquitylation and degradation, thus serving as activation-dependent negative-feedback regulators of cellular signaling. Although the role of CBL-C is unclear, mouse knockouts have revealed key physiological roles of CBL or CBL-B, individually as well as in combination, especially as negative regulators of immune responses and hematopoiesis (Duan et al., 2004; Mohapatra et al., 2013; Thien and Langdon, 2005). Relatively little is known about the role(s) of CBL proteins in mammalian epithelia despite their broad epithelial expression and apparent redundancy. In this study we used three complementary conditional mouse gene deletion models to reveal a novel and crucial requirement for CBL and CBL-B in the maintenance of MaSCs. Multiple lines of evidence support our conclusion.

Mammary epithelium-selective *Cbl/Cbl-b* DKO via floxed *Cbl* deletion with MMTV-Cre (Wagner et al., 1997) on a whole-body *Cbl-b* null background led to a significant block in MG development (Fig. 1A). Transplantation of MMTV-Cre DKO MECs demonstrated that the MG developmental block was not due to preclinical MPD driven by MMTV-Cre-induced DKO HSCs (An et al., 2015; Naramura et al., 2010) (Fig. S3B). No defect in MG development was seen in *Cbl* null or *Cbl-b* null mice, indicating that CBL and CBL-B play a redundant, cell-autonomous regulatory role in the mammary epithelium. Redundancy between CBL and CBL-B and a compensatory increase in the expression of family members,

Development (2017) 144, 1072-1086 doi:10.1242/dev.138164

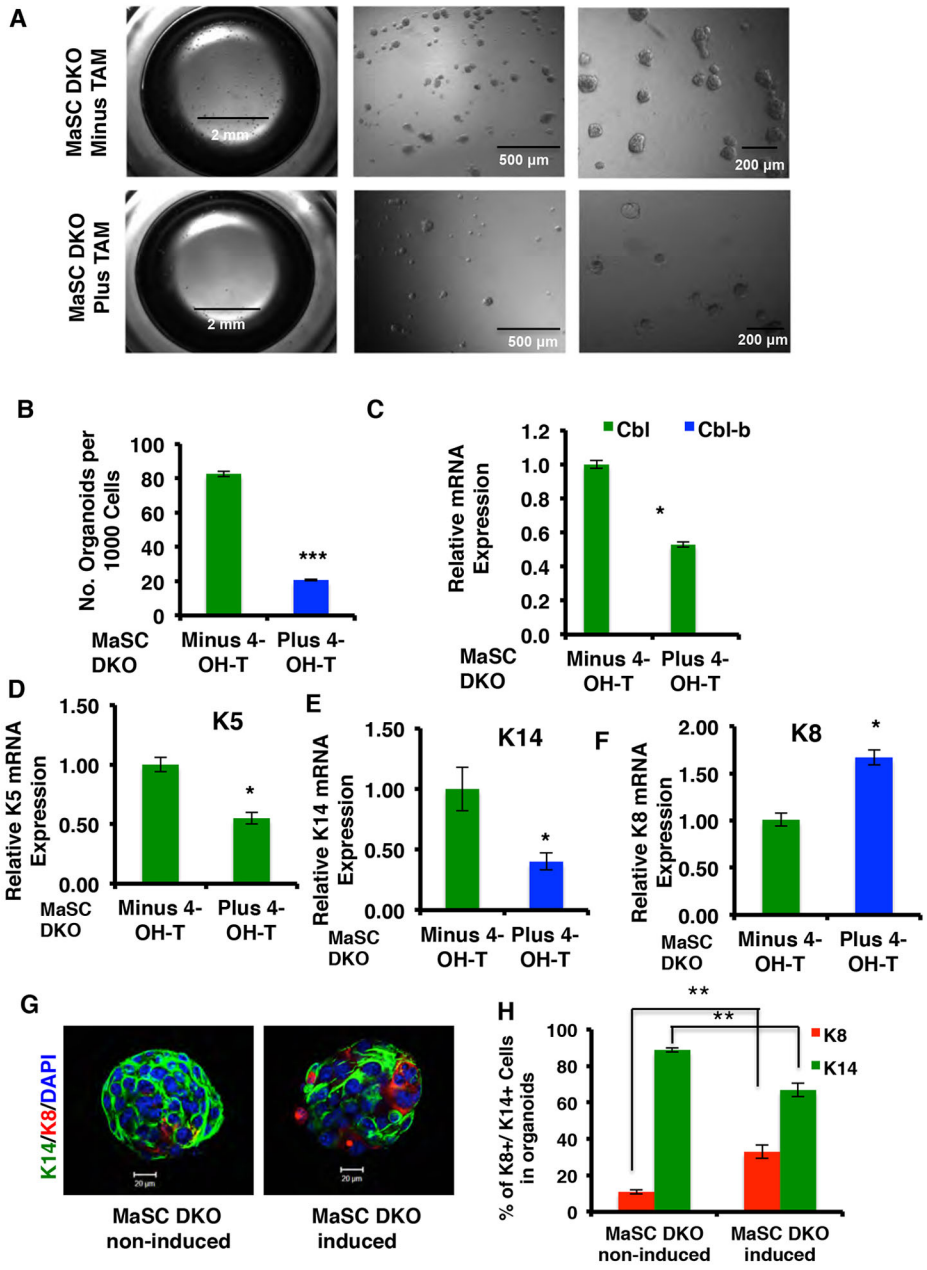

Fig. 6. Impairment of organoid-forming ability of Lgr5^{+} MECs isolated from Lgr5-CreERT-based conditional *Cbl/Cbl-b* DKO mice requires tamoxifen induction. Lgr5^{+} (GFP^{+}) cells were FACS sorted from *Lgr5-GFP-CreERT; Cbl$^{f/f}$; Cbl-b$^{-/-}$* mice and organoid cultures performed as in Fig. 5E,F for 9 days either without (A, top) or with (A, bottom) 4-OH-T. (B) Quantitation of organoid numbers as in A. (C) qPCR analysis verified 4-OH-T-induced reduction in *Cbl* expression and lack of *Cbl-b* expression in both non-induced and induced organoids. (D-G) qPCR (D-F) and immunofluorescence (G) analyses were performed to assess the expression of basal (K5, D; K14, E,G) and luminal (K8, F,G) cytokeratins. (H) Quantitation of immunofluorescence staining of basal and luminal cytokeratins in organoids as in G. Data (n=3) are shown as mean±s.e.m. *P≤0.05, **P≤0.01, ***P≤0.001 (Student's t-test).

as seen in *Cbl-b* null MGs (Fig. 1E), is likely to account for the lack of MG phenotypes in MGs of single-KO mice. Increased mammary branching as previously reported in *Cbl* null mice (Murphy et al., 1998) was later shown to be due to a non-cell-autonomous increase in growth factor secretion by the stroma (Crowley et al., 2005).

Surface marker-based analyses revealed a significant reduction in the overall numbers of MECs and their basal and luminal subsets in DKO mice, with a more substantial reduction in the MaSC-containing basal population, leading to a relative increase in the proportion of luminal cells (Fig. 2A-D). Interestingly, CD61/CD29-based MEC subset analysis indicated an increase in luminal progenitors but not the mature luminal cell pool. Together with a smaller basal population, this finding is consistent with a more rapid transition of DKO MaSCs into luminal progenitors. We suspect that such cells are functionally impaired since there was not a proportionate increase in mature luminal cells (Fig. 2G,H). Importantly, *in vitro* and *in vivo* assays on basal MECs derived from the MMTV-Cre-driven DKO mice demonstrated impaired MaSC self-renewal and ability to regenerate a MG.

The requirement of CBL and CBL-B for the maintenance of MaSCs was independently confirmed by selectively inducing *Cbl/Cbl-b* DKO in Lgr5^{+} MECs, which have recently been established as bi-potent MaSCs with MG-regenerating ability (Barker et al., 2007, 2013). Tamoxifen-induced, MaSC-specific *Cbl/Cbl-b* DKO led to a rapid depletion of Lgr5^{+} cells (Fig. 4B), with the redistribution of a significant proportion of the remaining Lgr5^{+} MECs into luminal compartment. The reduction in MaSC numbers and their apparent transition into luminal cells appear to represent an abnormally accelerated differentiation of MaSCs at the expense of their self-renewal, as demonstrated by organoid studies (Fig. 5A,B, E,F,H, Fig. 6A,B). *In vitro* deletion of *Cbl* and *Cbl-b* in basal MECs from *CreERT; Cbl$^{f/f}$; Cbl-b$^{f/f}$* mice also led to reduced organoid-forming ability, complementing results from the other models

Development (2017) 144, 1072-1086 doi:10.1242/dev.138164

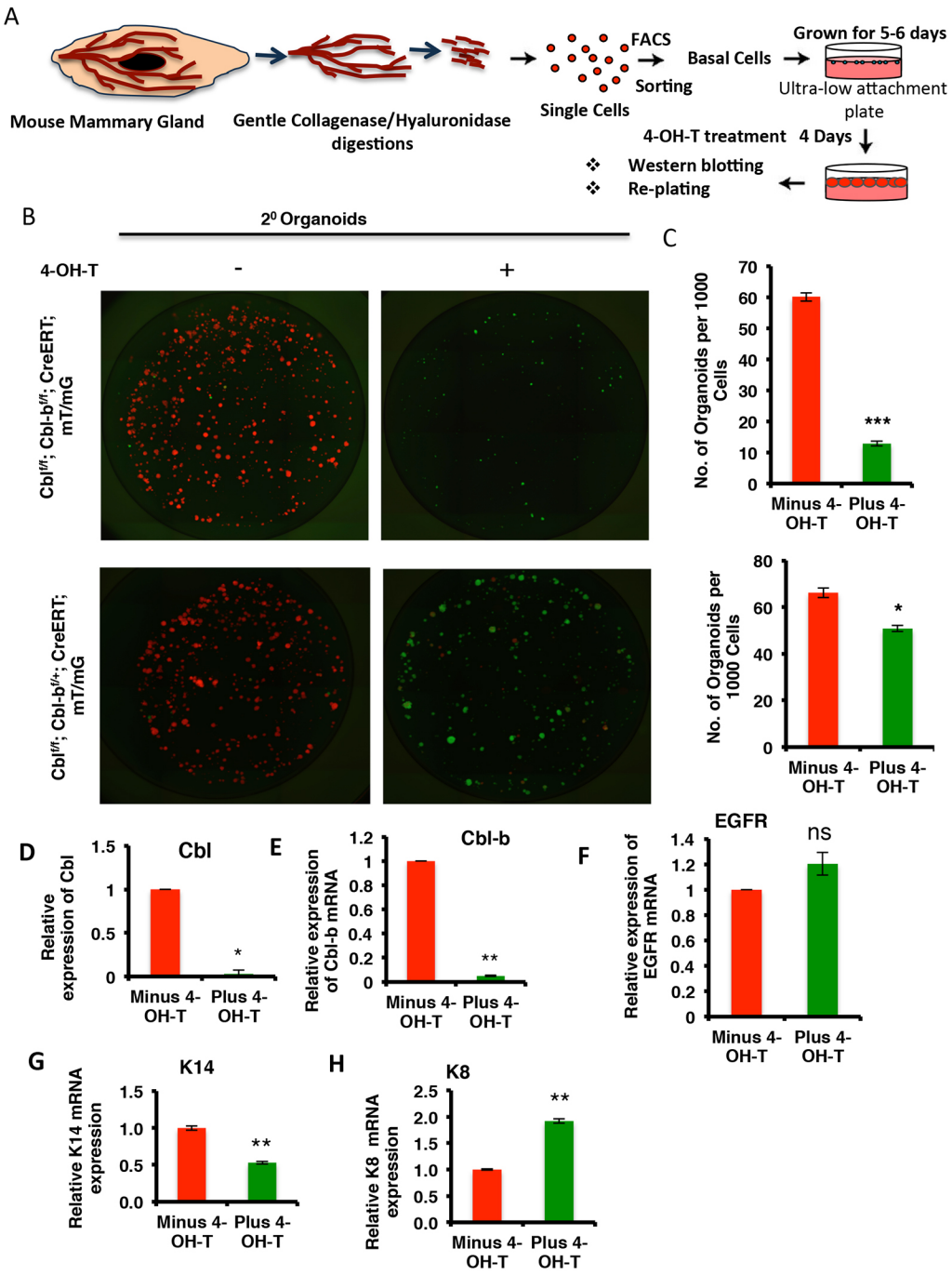

Fig. 7. Impaired stem cell renewal upon tamoxifen-induced, CreERT-mediated *in vitro* deletion in a *Cbl/Cbl-b* double-floxed model. (A) Schematic of basal MEC isolation from 8-week-old *Cbl$^{f/f}$; Cbl-b$^{f/f}$; CreERT; mT/mG* (conditional DKO) and *Cbl$^{f/f}$; Cbl-b$^{f/+}$; CreERT; mT/mG* (control) mice. Organoid cultures were established and treated with or without 4-OH-T to induce *Cbl/Cbl-b* deletion, tracked using a dual fluorescent reporter. (B,C) The non-induced or 4-OH-T-induced primary organoids formed by isolated basal cells from *Cbl$^{f/f}$; Cbl-b$^{f/f}$; CreERT; mT/mG* (conditional DKO) and *Cbl$^{f/f}$; Cbl-b$^{f/+}$; CreERT; mT/mG* (control) mice were replated (2° organoids) to assess self-renewal ability. (B) Representative images showing loss of red (RFP) and gain of green (GFP) fluorescence indicating successful CreERT activation and *Cbl/Cbl-b* deletion (confirmed by WB, not shown). (C) Quantitation of organoid numbers from B. Note the dramatic reduction in organoid numbers in 4-OH-T-treated double-floxed organoids only. (D-F) qPCR analyses verify the deletion of *Cbl* and *Cbl-b*, with no significant upregulation of *Egfr*. (G,H) Relative expression of basal (*K14*, G) and luminal (*K8*, H) cytokeratins in 4-OH-T-induced versus non-induced organoids following replating. Data (n=3) are shown as mean±s.e.m. ns, $P \geq 0.05$; *$P \leq 0.05$, **$P \leq 0.01$, ***$P \leq 0.001$ (Student's t-test).

(Fig. 7B,C). Although our immunofluorescence and qPCR analyses in multiple models support the idea of differentiation of MaSCs towards luminal lineages, mammary lineage tracing in *Cbl^{flox}/Cbl-b^{flox}* mice bearing the dual reporter, possibly using K14-Cre (Van Keymeulen and Blanpain, 2012; Visvader and Stingl, 2014), will be needed to definitively test this idea.

Since negative regulation of PTKs is the primary biochemical function of CBL family proteins (Mohapatra et al., 2013), we surmised that dysregulated signaling downstream of PTK-coupled receptors in MaSCs was responsible for the rapid MaSC depletion upon *Cbl* and *Cbl-b* deletion. As multiple potential CBL/CBL-B target RTKs, including ErbB receptors, c-MET, IGF1/2 receptors and FGF receptors, are known to regulate MG development (Gjorevski and Nelson, 2011; Hynes and Watson, 2010; Sternlicht, 2006), we focused on AKT-mTOR signaling because it is a pivotal signaling axis downstream of all RTKs and non-receptor PTKs (Sun and Bernards, 2014), and its hyperactivity is associated with stem cell exhaustion in hematopoietic, neural and epidermal stem cells (Iglesias-Bartolome et al., 2012; Kalaitzidis et al., 2012; Magri et al., 2011). Indeed, inducible CreERT-mediated *Cbl/Cbl-b* DKO demonstrated an upregulation of pAKT and pmTOR in addition to the expected increase in pEGFR and EGFR levels, as organoids are cultured in EGF (Fig. 8A). CBL/CBL-B proteins are well-established negative regulators of RTKs. We chose EGFR as an index RTK since the organoids are grown in the presence of EGF and FGF2. As the use of an EGFR inhibitor (or lack of addition of EGF in the culture medium) would make the organoid assay unfeasible, we focused on downstream signaling

Development (2017) 144, 1072-1086 doi:10.1242/dev.138164

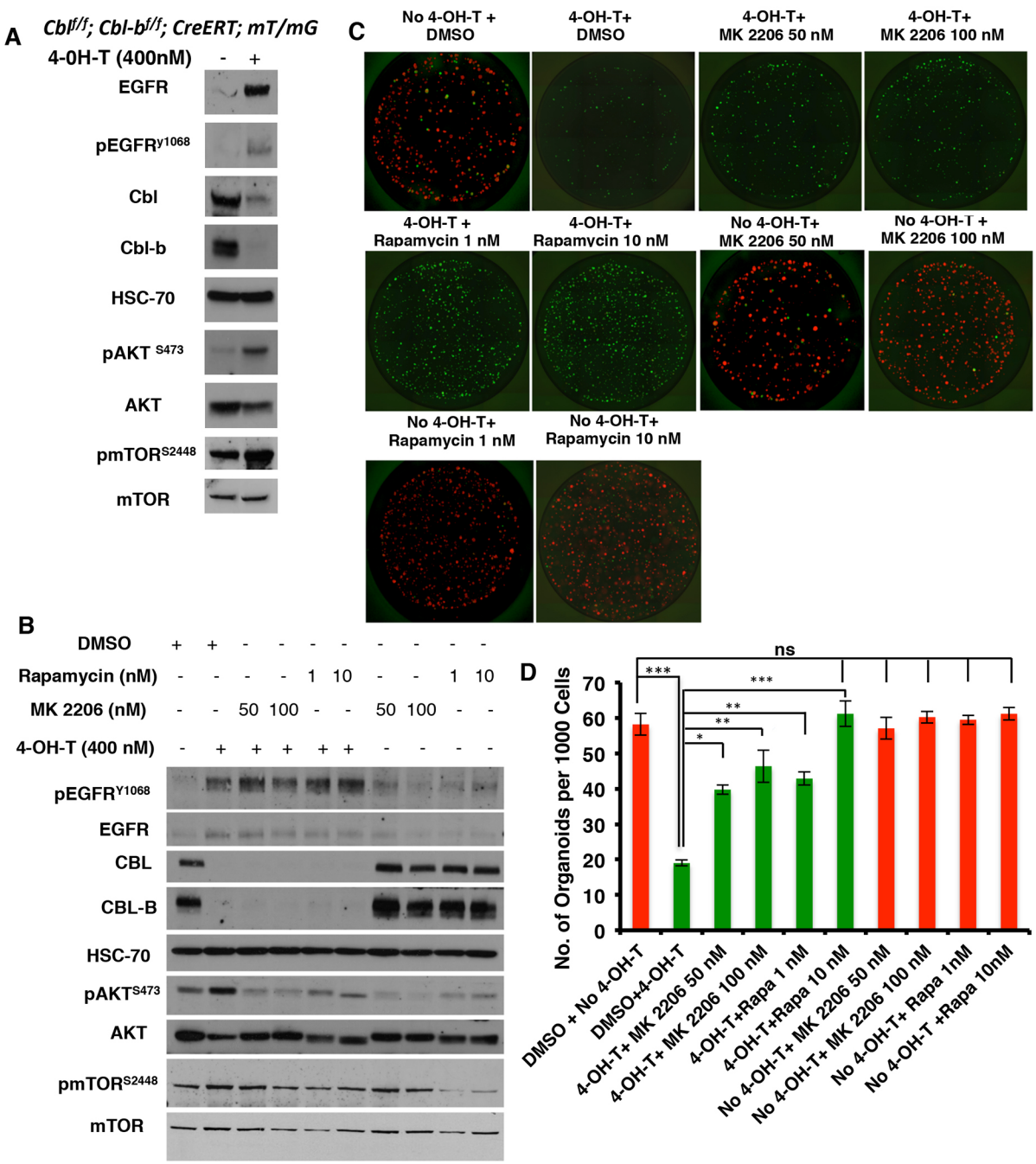

Fig. 8. Hyperactivation of AKT-mTOR signaling mediates loss of MaSC self-renewal ability upon conditional *Cbl*/*Cbl-b* deletion. (A) Basal mammary cells were isolated from 8-week-old *Cbl*$^{f/f}$*; Cbl-b*$^{f/f}$*; CreERT; mT/mG* mice, plated for organoid culture for 10 days with or without 4-OH-T for the last 4 days. WB of non-induced versus induced primary organoids which exhibit CBL/CBL-B deletion and an increase in the levels of total EGFR, pEGFR, pAKT and pmTOR. (B) Basal mammary cells plated for 10 days, with or without 4-OH tamoxifen or the inhibitors MK-2206 or rapamycin at the indicated concentrations for the last 4 days. WB demonstrates the reduction in pAKT or pmTOR levels as indicators of AKT or mTOR inhibition, respectively, after primary organoid culture. Rapamycin-induced loss of pAKT signals reflects the feedback loop. Anti-CBL/CBL-B blotting verified the expected deletions. (C) Representative scanned images of induced (GFP$^+$, green) and non-induced (RFP$^+$, red) secondary organoid cultures without or with the indicated inhibitor treatment in primary culture. (D) Quantification of the number of organoids formed by induced (green bars) versus non-induced (red bars) MaSCs and the reversal of the effect of *Cbl*/*Cbl-b* deletion by AKT or mTOR inhibition. Data (n=3) are shown as mean±s.e.m. ns, $P \geq 0.05$; *$P \leq 0.05$, **$P \leq 0.01$, ***$P \leq 0.001$ (Student's t-test).

pathways that are shared between RTKs activated by the added ligands as well as those that might be produced by MaSCs themselves. Our results raised the possibility that hyperactive mTOR signaling might commit *Cbl/Cbl-b* DKO MaSCs to premature differentiation, thereby reducing their self-renewing pool. A chemical inhibitor strategy supported such a role of hyperactive AKT-mTOR signaling. However, whether hyperactive mTOR is sufficient for MaSC depletion needs to be directly tested; our attempts to test this by expressing constitutively active or dominant-negative RHEB (Nie et al., 2010) were unsuccessful due to technical difficulties in lentiviral infection of primary organoids. The partial rescue of MaSC self-renewal by AKT inhibition versus an essentially complete rescue by mTOR inhibition (Fig. 8B-D) supports a model in which the hyperactivity of AKT and other

Development (2017) 144, 1072-1086 doi:10.1242/dev.138164

upstream signaling pathways increases mTOR signaling to deplete MaSCs by promoting their rapid differentiation. Among the upstream pathways that might add to increased mTOR activity, ERK is a likely candidate as it is hyperphosphorylated when *Cbl* and *Cbl-b* are genetically deleted in HSCs (An et al., 2015) or depleted by shRNA in human MECs (Duan et al., 2011). Culture of human mammary organoids with amphiregulin has been found to maintain MECs in a less differentiated state, whereas growth in EGF led to myoepithelial differentiation; this dichotomy was shown to be related to sustained ERK/RSK signaling by EGF (Pasic et al., 2011).

Although our results support the likelihood that hyperactive mTOR results in rapid differentiation and loss of MaSCs, it is possible that the increased differentiation is a consequence rather than a cause of MaSC depletion. In this context, CBL is unequally distributed in daughter cells of asymmetrically dividing neural stem cells, with higher CBL correlating with lower EGFR levels in daughter cells that retain stemness (Ferron et al., 2010). Future studies to investigate a potential role of CBL and CBL-B in promoting asymmetric division in MaSCs will therefore be of interest.

Conclusions

Our studies provide the first evidence for a cell-intrinsic and redundant requirement of CBL and CBL-B in epithelial stem cell self-renewal and maintenance, provide a mechanistic basis for this requirement and suggest that fine-tuning of mTOR signaling is crucial for MaSC maintenance. These insights, together with models generated here, should help uncover an unanticipated positive role of CBL family proteins in epithelial stem cell maintenance, with implications for epithelial stem cell biology and cancers.

MATERIALS AND METHODS

Antibodies

The following antibodies were used for WB: mouse monoclonal antibodies to CBL (clone 17/c-Cbl, BD Biosciences, 610442; 1:1000), HSC70 (clone B6, Santa Cruz, SC-7298; 1:10,000), cytokeratin 8 (Troma-1, Developmental Studies Hybridoma Bank; 1:200) and Ki67 (Alexa 488 conjugated, BD Biosciences, B56 clone, 558616; 1:200); rabbit monoclonal antibodies to CBL-B [clone D3C12, Cell Signaling Technology (CST), 9498; 1:1000], phospho-AKT (Ser473, CST, 4060; 1:500), pan-AKT (CST, 4691; 1:1000), phospho-mTOR (Ser2448, CST, 5536; 1:1000), mTOR (7C10, CST, 2983; 1:1000) and cyclin D1 (SP4, Abcam, ab16663; 1:200) and rabbit polyclonal antibodies to cytokeratin 5 (Covance, PRB-106P; 1:500), cytokeratin 14 (Covance, PRB-155P; 1:200), cleaved caspase 3 (CST, 9662; 1:200), EGFR (sc-03, Santa Cruz, 1005; 1:500) and phospho-EGF receptor (Tyr1068, CST, 2234; 1:1000). Anti-CD24-PE (clone M1/69, BD Biosciences, 553262; 1:50), anti-EpCAM-PE (eBioscience, 12-5791-82; 1:50), anti-CD29-APC (clone eBioHMb1-1, eBiosciences, 17-0291-82; 1:50) and anti-CD61-BV421 (clone 2C9.G2, BD Horizon, 562917; 1:50) were used for flow cytometry. Biotinylated anti-CD45 (clone 30-F11, BD Biosciences, 553077; 1:50), anti-Ter119 (clone ter119, BD Biosciences, 553672, 1:50) and anti-CD31 (clone MEC 13.3, BD Biosciences, 553371; 1:50) antibodies were used for AUTOMACS depletion of Lin^+ cells.

Media, reagents and chemicals

All reagents and media used for primary mammary epithelial isolation and *in vitro* organoid and mammosphere cultures were from Stem Cell Technologies, unless otherwise specified. ROCK inhibitor was from Tocris Bioscience. Tamoxifen, 4-OH-T, recombinant EGF, FGF and rapamycin (R0395) were from Sigma. MK-2206 2HCl was from Selleckchem (S1078). Reduced growth factor Matrigel was from BD Biosciences.

Mouse strains

Mice carrying MMTV-Cre [stock Tg(MMTV-Cre)4 Mam/J] for conditional floxed *Cbl* deletion ($Cbl^{tm2Hua}/Cbl^{f/f}$) (Naramura et al., 2010) on a *Cbl-b* null ($Cbl\text{-}b^{tm1Hua}$) background (*Cbl/Cbl-b* DKO) (all genotypes are listed in Table S1) as well as *Cbl* KO (Cbl^{tm1Hua}) (Naramura et al., 1998) and *Cbl-b* KO ($Cbl\text{-}b^{tm1Hua}$) (Chiang et al., 2000) mice have been described previously. *ROSA26* locus *lacZ* reporter [$B6.129S4\text{-}Gt(ROSA)26Sor^{tm1Sor/J}$] and *EGFP* reporter (*CAG-CAT-EGFP*) (Naramura et al., 2010) were incorporated to track cells with Cre-dependent target gene deletion. To generate a tamoxifen-inducible MaSC *Cbl/Cbl-b* DKO model, the *Lgr5-GFP-IRES-CreERT* allele (The Jackson Laboratory) was incorporated into $Cbl^{f/f}$; $Cbl\text{-}b^{-/-}$; *R26R-lacZ* mice. Control mice were littermates obtained during breeding. We engineered a $Cbl\text{-}b^{f/f}$ mouse model and used it to generate a $Cbl^{f/f}$; $Cbl\text{-}b^{f/f}$; *CreERT; mT/mG* strain that was used for *in vitro* *Cbl* and *Cbl-b* deletion in MaSCs in certain experiments (Goetz et al., 2016). Three-week-old female NSG mice (NOD.Cg-$Prkdc^{scid}$ $Il2rg^{tm1Wjl/SzJ}$) (The Jackson Laboratory) were used as recipients for mammary transplantation. All mouse strains were maintained on a C57BL/6J background under specific pathogen-free conditions and genotyped using tail DNA PCR (sequences are provided in Table S2). All experimental analyses were carried out on female mice. The Institutional Animal Care and Use Committee of University of Nebraska Medical Center approved all mouse experiments.

MG harvest and whole-mount staining

Fourth (inguinal) MGs were excised and processed according to a standard protocol (LaMarca and Rosen, 2007). Whole-mounts were photographed and various parameters (branch points, ductal length and fat pad filling) were quantified using Nikon Elements software. Whole MG X-gal staining, to visualize *lacZ*-encoded β-galactosidase activity as a reporter of gene deletion, was performed as described (LaMarca and Rosen, 2007). At least four animals were analyzed per genotype and time point.

Immunofluorescence analyses and western blotting (WB)

Staining of paraffin-embedded MG sections and mammary organoids with fluorescently labeled antibodies was carried out using standard protocols as previously described (Pasic et al., 2011). WB of freshly isolated MG and organoids was performed as described in the supplementary Materials and Methods.

Immunohistochemistry (IHC)

Formalin-fixed and paraffin-embedded tissue sections were stained with anti-CBL antibody using the Mouse on Mouse (MOM) and ABC Amplification IHC Kit (Vector Laboratories) as per the manufacturer's instructions. The slides were counterstained with Hematoxylin. In all cases, a species-matched (and isotype-matched for mouse monoclonal antibodies) control IgG was used as a negative control.

Transplantation assay

The mammary epithelial tissue between the nipple and lymph node of the fourth MG of 3-week-old immune-compromised NSG female mice was removed to yield epithelium-cleared fat pads (Deome et al., 1959). Complete removal of the mammary epithelium was verified by whole-mount staining. Recipient mice received a control mammary transplant on one side and a *Cbl/Cbl-b* DKO transplant on the contralateral side. The transplants were harvested from virgin hosts 8 weeks post-transplantation. Alternatively, the recipients were bred with fertile males and the glands harvested at various points of pregnancy. The whole-mounts of transplants were stained with carmine alum or X-gal.

MG repopulating activity

To test MG repopulating activity, 50,000 Lin^- single MECs isolated from 6-week-old DKO or control MGs were suspended in 100 µl 1:1 mix of Matrigel and Complete Mouse Epicult-B medium (STEMCELL Technologies, 05610) and then injected into epithelium-cleared mammary fat pads of 3-week-old NSG mice. In other experiments, 5000 Lin^-/$EpCAM^+$ cells were directly sorted into Epicult-B medium, centrifuged (400 ***g*** for 5 min at 4°C) and resuspended in 50 µl 1:1 Epicult-B medium and Matrigel, and injected into epithelium-cleared fat pads. Mammary fat pads were harvested 8 weeks after transplant and stained with carmine alum to assess the extent of mammary outgrowths.

Development (2017) 144, 1072-1086 doi:10.1242/dev.138164

Isolation of primary mouse MECs and flow cytometry

Single cells were prepared from mammary tissue as previously described (Stingl et al., 2006a,b). Single-cell suspensions were stained with a combination of biotinylated anti-CD45, anti-Ter119 and anti-CD31 antibodies followed by anti-biotin microbeads (Miltenyi Biotech) to magnetically deplete the Lin^+ cells using AUTOMACS (Miltenyi Biotech). Lin^- cells were co-stained with the indicated combinations of anti-CD24-PE, anti-EpCAM-PE, anti-CD29-APC and anti-CD61-BV421. FACS analysis and cell sorting were performed on a FACSAria II (BD Biosciences) and the results analyzed using FlowJo software.

In vivo Lgr5-Cre-mediated gene deletion

To induce Lgr5-CreERT-mediated floxed *Cbl* deletion *in vivo*, 4-week-old mice received three consecutive daily intraperitoneal injections of tamoxifen (1 mg/20 g body weight) in corn oil (10 mg/ml stock). Mice were analyzed at day 5 or 10 as indicated.

In vitro mammary epithelial organoid culture assay for MaSC renewal

In vitro mammary epithelial organoid culture was performed as described (Guo et al., 2012) with minor modifications. FACS sorting of single MECs was used to prepare the GFP^+ fraction from control or DKO mice carrying the *Lgr5-GFP-CreERT* allele, or the RFP^+ basal cell fraction from *Cbl$^{f/f}$; Cbl-b$^{f/f}$; CreERT; mT/mG* or *Cbl$^{f/f}$; Cbl-b$^{f/+}$; CreERT; mT/mG* (control) mice. Cells were seeded at 2000-5000 per well in 100% Matrigel in 8-well Lab-Tek plates (Nunc) precoated with Matrigel and fed with complete Epicult-B medium and 5 µM Y-27632 (ROCK inhibitor; TOCRIS, 1254). The medium was replaced every 2 days. Organoids (>100 µm in diameter) were imaged and counted 7-14 days after seeding. For immunofluorescence analyses, organoid cultures were fixed with 4% paraformaldehyde, permeabilized with 0.5% Triton X-100 in PBS and processed as described previously (Ewald et al., 2008).

Mammosphere assay of MaSC renewal

In vitro mammosphere assay of MaSC renewal was performed as described (Guo et al., 2012). GFP^+ basal ($CD29^{hi}$ $EpCAM^{low}$) and luminal ($CD29^{low}$ $EpCAM^{hi}$) cell populations from DKO and control mice carrying the *MMTV-Cre-GFP* allele or the GFP^+ fraction of single MECs from control or DKO mice carrying the *Lgr5-GFP-CreERT* allele, or the RFP^+ basal cells sorted from *Cbl$^{f/f}$; Cbl-b$^{f/f}$; CreERT; mT/mG* and *Cbl$^{f/f}$; Cbl-b$^{f/+}$; CreERT; mT/mG* (control) were prepared by FACS sorting and seeded in complete Epicult-B medium containing 5% Matrigel, as above, at 1000-2000 per well in 96-well ultra low-attachment plates (Corning). Mammospheres were imaged and counted (>100 µm in diameter) 7-10 days after seeding. For serial passaging, mammospheres were harvested using 5 mg/ml dispase I (Stem Cell Technologies) and dissociated in 0.25% trypsin-EDTA (Gibco). Single cells were seeded (2000 per well) for 7-10 days followed by imaging, counting, and further passaging of mammospheres.

In vitro Lgr5-Cre-mediated *Cbl* and *Cbl-b* deletion

Sorted GFP^+ MECs from *Cbl$^{fl/+}$; Cbl-b$^{+/-}$; Lgr5-CreERT* (control) or *Cbl$^{fl/fl}$; Cbl-b$^{-/-}$; Lgr5-CreERT* (DKO) mice were plated in 100% Matrigel in Matrigel-coated 8-well chambers and cultured in Epicult-B medium with ROCK inhibitor for 7 days (Guo et al., 2012). The medium was replaced every 2 days. For *in vitro* Cre activation, 400 nM 4-OH-T in Epicult-B medium was added for 96 h beginning at day 3, replaced with regular medium for 1 day, and organoids harvested. 2000 cells were then replated per well in 96-well ultra low-attachment plates to assess mammosphere-forming efficiency.

In vitro Rosa26-CreERT induction and inhibitor treatment

RFP^+ basal and luminal cells were isolated from *Cbl$^{fl/f}$; Cbl-b$^{f/f}$; CreERT; mT/mG* and *Cbl$^{fl/f}$; Cbl-b$^{f/+}$; CreERT; mT/mG* mice and plated in 96-well ultra low-attachment plates for 7 days as described above. 400 nM 4-OH-T was added in Epicult-B medium for 96 h. GFP expression in organoids indicates induction of Cre and deletion of floxed genes. WBs were performed to test the signaling events and CBL and CBL-B deletion. Basal organoids were treated with MK-2206 (50 nM, 100 nM) or rapamycin (1 nM, 10 nM) with and without 4-OH-T induction for 4 days. Single cells were replated, and organoids imaged and quantified. Non-induced cultures were treated with inhibitors alone to control for any non-specific effects. DMSO was used as a vehicle control.

Real-time quantitative PCR (qPCR)

FACS-sorted cells were directly collected in Trizol reagent (Ambion, Life Technologies) for RNA extraction. Detailed procedures are provided in the supplementary Materials and Methods and qPCR primers are listed in Table S3.

Statistical analyses

Quantified results of whole-mounts, qPCR, IHC and flow cytometry were compared between groups using Student's *t*-test and are presented as mean±s.e.m., with $P \leq 0.05$ deemed significant. Statistical analysis and graphical representation of data were performed using Prism 4.0c (GraphPad).

Acknowledgements

We thank the H.B. laboratory members for helpful discussions, Kay-Uwe Wagner and Aleata Triplett for advice on mammary transplants, the staff of UNMC Cores for assistance and Dr Andrew Ewald (Johns Hopkins School of Medicine) for sharing his protocol for mammary organoid staining.

Competing interests

The authors declare no competing or financial interests.

Author contributions

B.M., N.Z.: conceptualization and design, collection and/or assembly of data, data analysis and interpretation, manuscript writing; W.A., B.G., P.A., T.A.B., I.M., M.D.S.: collection and assembly of data, data analysis and interpretation, manuscript editing; J.L.M.: data analysis and interpretation; V.B.: conceptualization and design, manuscript editing; H.B.: conception and design, data analysis and interpretation, manuscript writing.

Funding

This work was supported by the National Institutes of Health (CA105489, CA87986, CA99163 to H.B.; CA96844, CA144027 to V.B.); the U.S. Department of Defense (W81WH-11-1-0167 to H.B.; W81XWH-07-1-0351, W81XWH-11-1-0171 to V.B.); the Nebraska Department of Health and Human Services LB606 (18123-Y3 to H.B.); an Institutional Development Award (IDeA) from the National Institute of General Medical Sciences (P30 GM106397); and a National Cancer Institute Core Support Grant (P30CA036727) to the Fred & Pamela Buffett Cancer Center and Nebraska Research Initiative. We thank the Dr Raphael Bonita Fund for partial support of graduate students W.A. and B.G. in the H.B. lab. B.M., N.Z., W.A. and P.A. received University of Nebraska Medical Center graduate assistantships. B.G. was a trainee under the National Cancer Institute Cancer Biology Training Grant. Deposited in PMC for release after 12 months.

Supplementary information

Supplementary information available online at
http://dev.biologists.org/lookup/doi/10.1242/dev.138164.supplemental

References

An, W., Nadeau, S. A., Mohapatra, B. C., Feng, D., Zutshi, N., Storck, M. D., Arya, P., Talmadge, J. E., Meza, J. L., Band, V. et al. (2015). Loss of Cbl and Cbl-B ubiquitin ligases abrogates hematopoietic stem cell quiescence and sensitizes leukemic disease to chemotherapy. *Oncotarget* **6**, 10498-10509.

Ballou, L. M. and Lin, R. Z. (2008). Rapamycin and mTOR kinase inhibitors. *J. Chem. Biol.* **1**, 27-36.

Barker, N., van Es, J. H., Kuipers, J., Kujala, P., van den Born, M., Cozijnsen, M., Haegebarth, A., Korving, J., Begthel, H., Peters, P. J. et al. (2007). Identification of stem cells in small intestine and colon by marker gene Lgr5. *Nature* **449**, 1003-1007.

Barker, N., Tan, S. and Clevers, H. (2013). Lgr proteins in epithelial stem cell biology. *Development* **140**, 2484-2494.

Beck, B. and Blanpain, C. (2013). Unravelling cancer stem cell potential. *Nat. Rev. Cancer* **13**, 727-738.

Brisken, C., Heineman, A., Chavarria, T., Elenbaas, B., Tan, J., Dey, S. K., McMahon, J. A., McMahon, A. P. and Weinberg, R. A. (2000). Essential function of Wnt-4 in mammary gland development downstream of progesterone signaling. *Genes Dev.* **14**, 650-654.

Cai, C., Yu, Q. C., Jiang, W., Liu, W., Song, W., Yu, H., Zhang, L., Yang, Y. and Zeng, Y. A. (2014). R-Spondin1 is a novel hormone mediator for mammary stem cell self-renewal. *Genes Dev.* **28**, 2205-2218.

Carr, J. R., Kiefer, M. M., Park, H. J., Li, J., Wang, Z., Fontanarosa, J., DeWaal, D., Kopanja, D., Benevolenskaya, E. V., Guzman, G. et al. (2012). FoxM1 regulates mammary luminal cell fate. *Cell Rep.* **1**, 715-729.

Chiang, Y. J., Kole, H. K., Brown, K., Naramura, M., Fukuhara, S., Hu, R. J., Jang, I. K., Gutkind, J. S., Shevach, E. and Gu, H. (2000). Cbl-B regulates the CD28 dependence of T-cell activation. *Nature* **403**, 216-220.

Crowley, M. R., Bowtell, D. and Serra, R. (2005). TGF-beta, c-Cbl, and PDGFR-alpha the in mammary stroma. *Dev. Biol.* **279**, 58-72.

de Visser, K. E., Ciampricotti, M., Michalak, E. M., Tan, D. W., Speksnijder, E. N., Hau, C. S., Clevers, H., Barker, N. and Jonkers, J. (2012). Developmental stage-specific contribution of LGR5(+)cells to basal and luminal epithelial lineages in the postnatal mammary gland. *J. Pathol.* **228**, 300-309.

Deome, K. B., Faulkin, L. J., Jr, Bern, H. A. and Blair, P. B. (1959). Development of mammary tumors from hyperplastic alveolar nodules transplanted into gland-free mammary fat pads of female C3H mice. *Cancer Res.* **19**, 515-520.

Dontu, G., Abdallah, W. M., Foley, J. M., Jackson, K. W., Clarke, M. F., Kawamura, M. J. and Wicha, M. S. (2003). In Vitro Propagation and transcriptional profiling of human mammary stem/progenitor cells. *Genes Dev.* **17**, 1253-1270.

Duan, L., Reddi, A. L., Ghosh, A., Dimri, M. and Band, H. (2004). The Cbl family and other ubiquitin ligases: destructive forces in control of antigen receptor signaling. *Immunity* **21**, 7-17.

Duan, L., Raja, S. M., Chen, G., Virmani, S., Williams, S. H., Clubb, R. J., Mukhopadhyay, C., Rainey, M. A., Ying, G., Dimri, M. et al. (2011). Negative regulation of EGFR-Vav2 signaling axis by Cbl ubiquitin ligase controls EGF receptor-mediated epithelial cell adherens junction dynamics and cell migration. *J. Biol. Chem.* **286**, 620-633.

Ewald, A. J., Brenot, A., Duong, M., Chan, B. S. and Werb, Z. (2008). Collective epithelial migration and cell rearrangements drive mammary branching morphogenesis. *Dev. Cell* **14**, 570-581.

Fang, D. and Liu, Y.-C. (2001). Proteolysis-independent regulation of PI3K by Cbl-B-mediated ubiquitination in T cells. *Nat. Immunol.* **2**, 870-875.

Ferron, S. R., Pozo, N., Laguna, A., Aranda, S., Porlan, E., Moreno, M., Fillat, C., de la Luna, S., Sánchez, P., Arbones, M. L. et al. (2010). Regulated segregation of kinase Dyrk1A during asymmetric neural stem cell division is critical for EGFR-mediated biased signaling. *Cell Stem Cell* **7**, 367-379.

Gjorevski, N. and Nelson, C. M. (2011). Integrated morphodynamic signalling of the mammary gland. *Nat. Rev. Mol. Cell Biol.* **12**, 581-593.

Goetz, B., An, W., Mohapatra, B., Zutshi, N., Iseka, F., Storck, M. D., Meza, J., Sheinin, Y., Band, V. and Band, H. (2016). A novel CBL-Bflox/flox mouse model allows tissue-selective fully conditional CBL/CBL-B double-knockout: CD4-Cre mediated CBL/CBL-B deletion occurs in both T-cells and hematopoietic stem cells. *Oncotarget* **7**, 51107-51123.

Griffiths, E. K., Sanchez, O., Mill, P., Krawczyk, C., Hojilla, C. V., Rubin, E., Nau, M. M., Khokha, R., Lipkowitz, S., Hui, C. C. et al. (2003). Cbl-3-deficient mice exhibit normal epithelial development. *Mol. Cell. Biol.* **23**, 7708-7718.

Guo, W., Keckesova, Z., Donaher, J. L., Shibue, T., Tischler, V., Reinhardt, F., Itzkovitz, S., Noske, A., Zürrer-Härdi, U., Bell, G. et al. (2012). Slug and Sox9 cooperatively determine the mammary stem cell state. *Cell* **148**, 1015-1028.

Hirai, H., Sootome, H., Nakatsuru, Y., Miyama, K., Taguchi, S., Tsujioka, K., Ueno, Y., Hatch, H., Majumder, P. K., Pan, B.-S. et al. (2010). MK-2206, an allosteric Akt inhibitor, enhances antitumor efficacy by standard chemotherapeutic agents or molecular targeted drugs in vitro and in vivo. *Mol. Cancer. Ther.* **9**, 1956-1967.

Humphreys, R. C., Krajewska, M., Krnacik, S., Jaeger, R., Weiher, H., Krajewski, S., Reed, J. C. and Rosen, J. M. (1996). Apoptosis in the terminal endbud of the murine mammary gland: a mechanism of ductal morphogenesis. *Development* **122**, 4013-4022.

Hynes, N. E. and Watson, C. J. (2010). Mammary gland growth factors: roles in normal development and in cancer. *Cold Spring Harb. Perspect. Biol.* **2**, a003186.

Iglesias-Bartolome, R., Patel, V., Cotrim, A., Leelahavanichkul, K., Molinolo, A. A., Mitchell, J. B. and Gutkind, J. S. (2012). mTOR inhibition prevents epithelial stem cell senescence and protects from radiation-induced mucositis. *Cell Stem Cell* **11**, 401-414.

Kalaitzidis, D., Sykes, S. M., Wang, Z., Punt, N., Tang, Y., Ragu, C., Sinha, A. U., Lane, S. W., Souza, A. L., Clish, C. B. et al. (2012). mTOR complex 1 plays critical roles in hematopoiesis and Pten-loss-evoked leukemogenesis. *Cell Stem Cell* **11**, 429-439.

Kessenbrock, K., Dijkgraaf, G. J. P., Lawson, D. A., Littlepage, L. E., Shahi, P., Pieper, U. and Werb, Z. (2013). A role for matrix metalloproteinases in regulating mammary stem cell function via the wnt signaling pathway. *Cell Stem Cell* **13**, 300-313.

Kitaura, Y., Jang, I. K., Wang, Y., Han, Y.-C., Inazu, T., Cadera, E. J., Schlissel, M., Hardy, R. R. and Gu, H. (2007). Control of the B cell-intrinsic tolerance programs by ubiquitin ligases Cbl and Cbl-b. *Immunity* **26**, 567-578.

Korkaya, H., Paulson, A., Iovino, F. and Wicha, M. S. (2008). HER2 regulates the mammary stem/progenitor cell population driving tumorigenesis and invasion. *Oncogene* **27**, 6120-6130.

LaMarca, H. L. and Rosen, J. M. (2007). Estrogen regulation of mammary gland development and breast cancer: amphiregulin takes center stage. *Breast Cancer Res.* **9**, 304.

Lim, E., Vaillant, F., Wu, D., Forrest, N. C., Pal, B., Hart, A. H., Asselin-Labat, M.-L., Gyorki, D. E., Ward, T., Partanen, A. et al. (2009). Aberrant luminal progenitors as the candidate target population for basal tumor development in BRCA1 mutation carriers. *Nat. Med.* **15**, 907-913.

Lim, E., Wu, D., Pal, B., Bouras, T., Asselin-Labat, M.-L., Vaillant, F., Yagita, H., Lindeman, G. J., Smyth, G. K. and Visvader, J. E. (2010). Transcriptome analyses of mouse and human mammary cell subpopulations reveal multiple conserved genes and pathways. *Breast Cancer Res.* **12**, R21.

Magri, L., Cambiaghi, M., Cominelli, M., Alfaro-Cervello, C., Cursi, M., Pala, M., Bulfone, A., Garcìa-Verdugo, J. M., Leocani, L., Minicucci, F. et al. (2011). Sustained activation of mTOR pathway in embryonic neural stem cells leads to development of tuberous sclerosis complex-associated lesions. *Cell Stem Cell* **9**, 447-462.

McCaffrey, L. M. and Macara, I. G. (2009). The Par3/aPKC interaction is essential for end bud remodeling and progenitor differentiation during mammary gland morphogenesis. *Genes Dev.* **23**, 1450-1460.

Mohapatra, B., Ahmad, G., Nadeau, S., Zutshi, N., An, W., Scheffe, S., Dong, L., Feng, D., Goetz, B., Arya, P. et al. (2013). Protein tyrosine kinase regulation by ubiquitination: critical roles of Cbl-family ubiquitin ligases. *Biochim. Biophys. Acta* **1833**, 122-139.

Murphy, M. A., Schnall, R. G., Venter, D. J., Barnett, L., Bertoncello, I., Thien, C. B., Langdon, W. Y. and Bowtell, D. D. L. (1998). Tissue hyperplasia and enhanced T-cell signalling via ZAP-70 in C-Cbl-deficient mice. *Mol. Cell. Biol.* **18**, 4872-4882.

Naramura, M., Kole, H. K., Hu, R. J. and Gu, H. (1998). Altered thymic positive selection and intracellular signals in Cbl-deficient mice. *Proc. Natl. Acad. Sci. USA* **95**, 15547-15552.

Naramura, M., Jang, I.-K., Kole, H., Huang, F., Haines, D. and Gu, H. (2002). C-Cbl and Cbl-B regulate T cell responsiveness by promoting ligand-induced TCR down-modulation. *Nat. Immunol.* **3**, 1192-1199.

Naramura, M., Nandwani, N., Gu, H., Band, V. and Band, H. (2010). Rapidly fatal myeloproliferative disorders in mice with deletion of casitas B-cell lymphoma (Cbl) and Cbl-B in hematopoietic stem cells. *Proc. Natl. Acad. Sci. USA* **107**, 16274-16279.

Nguyen, L. V., Vanner, R., Dirks, P. and Eaves, C. J. (2012). Cancer stem cells: an evolving concept. *Nat. Rev. Cancer* **12**, 133-143.

Nie, D., Di Nardo, A., Han, J. M., Baharanyi, H., Kramvis, I., Huynh, T. T., Dabora, S., Codeluppi, S., Pandolfi, P. P., Pasquale, E. B. et al. (2010). Tsc2-Rheb signaling regulates EphA-mediated axon guidance. *Nat. Neurosci.* **13**, 163-172.

Pasic, L., Eisinger-Mathason, T. S. K., Velayudhan, B. T., Moskaluk, C. A., Brenin, D. R., Macara, I. G. and Lannigan, D. A. (2011). Sustained activation of the HER1-ERK1/2-RSK signaling pathway controls myoepithelial cell fate in human mammary tissue. *Genes Dev.* **25**, 1641-1653.

Pece, S., Tosoni, D., Confalonieri, S., Mazzarol, G., Vecchi, M., Ronzoni, S., Bernard, L., Viale, G., Pelicci, P. G. and Di Fiore, P. P. (2010). Biological and molecular heterogeneity of breast cancers correlates with their cancer stem cell content. *Cell* **140**, 62-73.

Plaks, V., Brenot, A., Lawson, D. A., Linnemann, J. R., Van Kappel, E. C., Wong, K. C., de Sauvage, F., Klein, O. D. and Werb, Z. (2013). Lgr5-expressing cells are sufficient and necessary for postnatal mammary gland organogenesis. *Cell Rep.* **3**, 70-78.

Pond, A. C., Bin, X., Batts, T., Roarty, K., Hilsenbeck, S. and Rosen, J. M. (2013). Fibroblast growth factor receptor signaling is essential for normal mammary gland development and stem cell function. *Stem Cells* **31**, 178-189.

Rios, A. C., Fu, N. Y., Lindeman, G. J. and Visvader, J. E. (2014). In situ identification of bipotent stem cells in the mammary gland. *Nature* **506**, 322-327.

Robinson, G. W., Wagner, K. U. and Hennighausen, L. (2001). Functional mammary gland development and oncogene-induced tumor formation are not affected by the absence of the retinoblastoma gene. *Oncogene* **20**, 7115-7119.

Sangai, T., Akcakanat, A., Chen, H., Tarco, E., Wu, Y., Do, K.-A., Miller, T. W., Arteaga, C. L., Mills, G. B., Gonzalez-Angulo, A. M. et al. (2012). Biomarkers of response to Akt inhibitor MK-2206 in breast cancer. *Clin. Cancer Res.* **18**, 5816-5828.

Sarbassov, D. D., Ali, S. M., Sengupta, S., Sheen, J.-H., Hsu, P. P., Bagley, A. F., Markhard, A. L. and Sabatini, D. M. (2006). Prolonged rapamycin treatment inhibits mTORC2 assembly and Akt/PKB. *Mol. Cell* **22**, 159-168.

Shackleton, M., Vaillant, F., Simpson, K. J., Stingl, J., Smyth, G. K., Asselin-Labat, M.-L., Wu, L., Lindeman, G. J. and Visvader, J. E. (2006). Generation of a functional mammary gland from a single stem cell. *Nature* **439**, 84-88.

Shehata, M., Teschendorff, A., Sharp, G., Novcic, N., Russell, I. A., Avril, S., Prater, M., Eirew, P., Caldas, C., Watson, C. J. et al. (2012). Phenotypic and functional characterisation of the luminal cell hierarchy of the mammary gland. *Breast Cancer Res.* **14**, R134.

Siegel, P. M. and Muller, W. J. (2010). Transcription factor regulatory networks in mammary epithelial development and tumorigenesis. *Oncogene* **29**, 2753-2759.

Smalley, M. J., Kendrick, H., Sheridan, J. M., Regan, J. L., Prater, M. D., Lindeman, G. J., Watson, C. J., Visvader, J. E. and Stingl, J. (2012). Isolation of

mouse mammary epithelial subpopulations: a comparison of leading methods. *J. Mammary Gland Biol. Neoplasia* **17**, 91-97.

Soady, K. J., Kendrick, H., Gao, Q., Tutt, A., Zvelebil, M., Ordonez, L. D., Quist, J., Tan, D. W., Isacke, C. M., Grigoriadis, A. et al. (2015). Mouse mammary stem cells express prognostic markers for triple-negative breast cancer. *Breast Cancer Res.* **17**, 31.

Sternlicht, M. D. (2006). Key stages in mammary gland development: the cues that regulate ductal branching morphogenesis. *Breast Cancer Res.* **8**, 201.

Stingl, J., Eirew, P., Ricketson, I., Shackleton, M., Vaillant, F., Choi, D., Li, H. I. and Eaves, C. J. (2006a). Purification and unique properties of mammary epithelial stem cells. *Nature* **439**, 993-997.

Stingl, J., Raouf, A., Eirew, P. and Eaves, C. J. (2006b). Deciphering the mammary epithelial cell hierarchy. *Cell Cycle* **5**, 1519-1522.

Sun, C. and Bernards, R. (2014). Feedback and redundancy in receptor tyrosine kinase signaling: relevance to cancer therapies. *Trends Biochem. Sci.* **39**, 465-474.

Thien, C. B. F. and Langdon, W. Y. (2005). c-Cbl and Cbl-b ubiquitin ligases: substrate diversity and the negative regulation of signalling responses. *Biochem. J.* **391**, 153-166.

van Amerongen, R., Bowman, A. N. and Nusse, R. (2012). Developmental stage and time dictate the fate of Wnt/beta-catenin-responsive stem cells in the mammary gland. *Cell Stem Cell* **11**, 387-400.

Van Keymeulen,, A. and Blanpain, C. (2012). Tracing epithelial stem cells during development, homeostasis, and repair. *J. Cell Biol.* **197**, 575-584.

Visvader, J. E. (2009). Keeping abreast of the mammary epithelial hierarchy and breast tumorigenesis. *Genes Dev.* **23**, 2563-2577.

Visvader, J. E. and Stingl, J. (2014). Mammary stem cells and the differentiation hierarchy: current status and perspectives. *Genes Dev.* **28**, 1143-1158.

Wagner, K.-U., Wall, R. J., St-Onge, L., Gruss, P., Wynshaw-Boris, A., Garrett, L., Li, M., Furth, P. A. and Hennighausen, L. (1997). Cre-mediated gene deletion in the mammary gland. *Nucleic Acids Res.* **25**, 4323-4330.

Wang, Y., Dong, J., Li, D., Lai, L., Siwko, S., Li, Y. and Liu, M. (2013). Lgr4 regulates mammary gland development and stem cell activity through the pluripotency transcription factor Sox2. *Stem Cells* **31**, 1921-1931.

Weichhart, T., Hengstschlager, M. and Linke, M. (2015). Regulation of innate immune cell function by mTOR. *Nat. Rev. Immunol.* **15**, 599-614.

Yamaji, D., Na, R., Feuermann, Y., Pechhold, S., Chen, W., Robinson, G. W. and Hennighausen, L. (2009). Development of mammary luminal progenitor cells is controlled by the transcription factor STAT5A. *Genes Dev.* **23**, 2382-2387.

Yap, T. A., Yan, L., Patnaik, A., Fearen, I., Olmos, D., Papadopoulos, K., Baird, R. D., Delgado, L., Taylor, A., Lupinacci, L. et al. (2011). First-in-man clinical trial of the oral pan-AKT inhibitor MK-2206 in patients with advanced solid tumors. *J. Clin. Oncol.* **29**, 4688-4695.

Zeng, Y. A. and Nusse, R. (2010). Wnt proteins are self-renewal factors for mammary stem cells and promote their long-term expansion in culture. *Cell Stem Cell* **6**, 568-577.

Supplementary Materials and Methods

Lysate preparation and western blotting

Freshly excised mammary glands were snap frozen in liquid nitrogen and homogenized using a Pro-Scientific homogenizer in RIPA lysis buffer (50 mM Tris chloride pH 7.5, 100 mM NaF, 0.1% SDS, 1 mM EDTA, 1 mM PMSF, 10 µg/ml Aprotinin, 10 µg/ml Leupeptin, 1 mM Na3VO4, and 0.02% NP-40) (Sakamoto et al., 2007). Mammary organoid lysates were prepared in the same lysis buffer. Lysates were resolved on 8-10% SDS-PAGE and transferred to PVDF membranes, which were blocked with 2% BSA in Tris-buffered saline (TBS) and incubated overnight at 4°C with specific antibodies diluted in TBS-T (TBS, 0.1% Tween-20). Membranes were washed three times in TBS-T, incubated with HRP-conjugated species-specific secondary antibodies (Zymed Laboratories) and signals were detected with Pierce ECL substrate (Thermo Scientific).

Real-time quantitative PCR (qPCR)

FACS-sorted cells were directly collected in Trizol reagent (Ambion, Life Technology) for RNA extraction. cDNA was obtained by reverse transcription using the Invitrogen SuperScript III system (18080-051), and real-time qPCR was done using the SYBR Green labeling method (Applied Biosystems; 4309155) on a Bio-Rad CFX-96 Thermo Cycler. Primer sequences (Sigma-Aldrich) are listed in Table S3. Relative gene expression was calculated according to the ΔCt method, and normalized to Gapdh reference gene expression. A representative of three independent cell-sorting experiments is presented.

References

Sakamoto, K., Creamer, B. A., Triplett, A. A. and Wagner, K. U. (2007). The Janus Kinase 2 is Required for Expression and Nuclear Accumulation of Cyclin D1 in Proliferating Mammary Epithelial Cells. *Mol. Endocrinol.* **21**, 1877-1892.

Naramura, M., Nandwani, N., Gu, H., Band, V. and Band, H. (2010). Rapidly Fatal Myeloproliferative Disorders in Mice with Deletion of Casitas B-Cell Lymphoma (Cbl) and Cbl-B in Hematopoietic Stem Cells. *Proc. Natl. Acad. Sci. U. S. A.* **107**, 16274-16279.

Wagner, K. U., McAllister, K., Ward, T., Davis, B., Wiseman, R. and Hennighausen, L. (2001). Spatial and Temporal Expression of the Cre Gene Under the Control of the MMTV-LTR in Different Lines of Transgenic Mice. *Transgenic Res.* **10**, 545-553.

Supplementary Figures:

A.

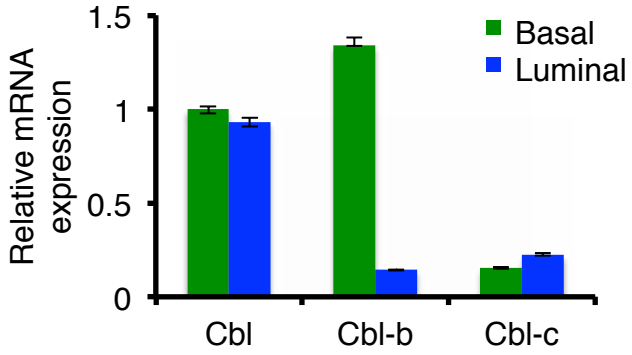

B.

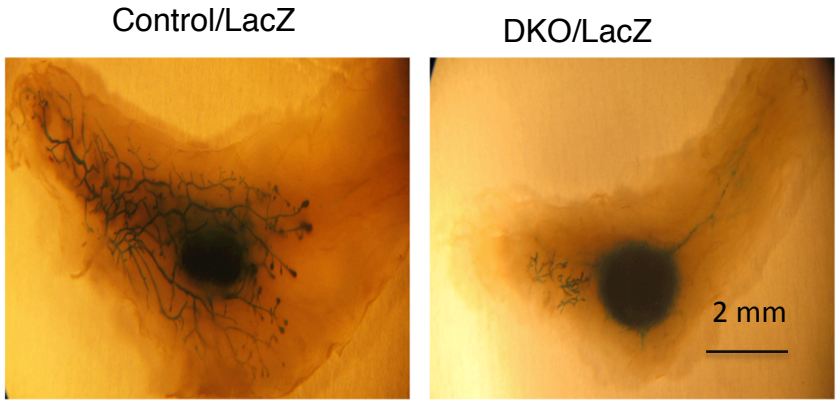

C.

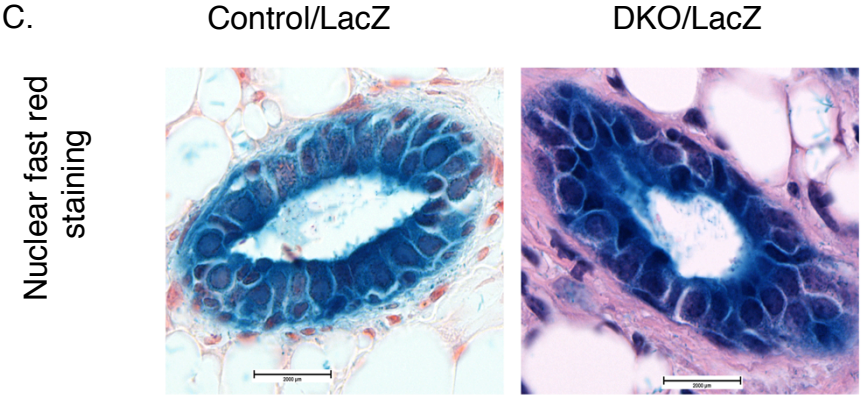

D.

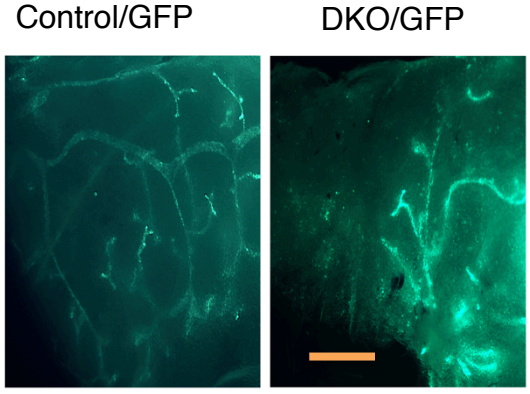

Figure S1. Quantitative PCR analysis of the expression of CBL family members in mammary epithelial cells and verification of MMTV-Cre-mediated recombination in *Cbl/Cbl-b* DKO mammary glands using reporter genes. (A) Real time quantitative PCR (qPCR) using primer sets specific for CBL, CBL-B or CBL-C was performed on mRNA isolated from FACS-isolated basal ($CD29^{hi}EpCAM^{low}$) and luminal ($CD29^{low}EpCAM^{hi}$) compartments of normal mouse mammary gland. Values are expressed relative to GAPDH, used as an internal reference. Data shown are mean +/- SEM, n=3. (B) Mammary glands of 6-week old *Cbl/Cbl-b* DKO and control mice carrying a LacZ reporter allele were stained with x-gal to visualize the distribution of β-galactosidase activity, which is seen in the epithelium and not the stroma. Staining of lymph node is due to concurrent deletion in the hematopoietic system, as previously described (Naramura et al., 2010;Wagner et al., 2001). (C) Nuclear fast red (counterstains nuclei as pink) and X-gal staining was performed to reveal MMTV-Cre-mediated targeted gene deletion in both luminal and basal compartments. (D) Fluorescent microscopy analysis to visualize GFP expression in the mammary ducts of DKO and control mice carrying a GFP reporter allele. Scale bar represents 500 μM.

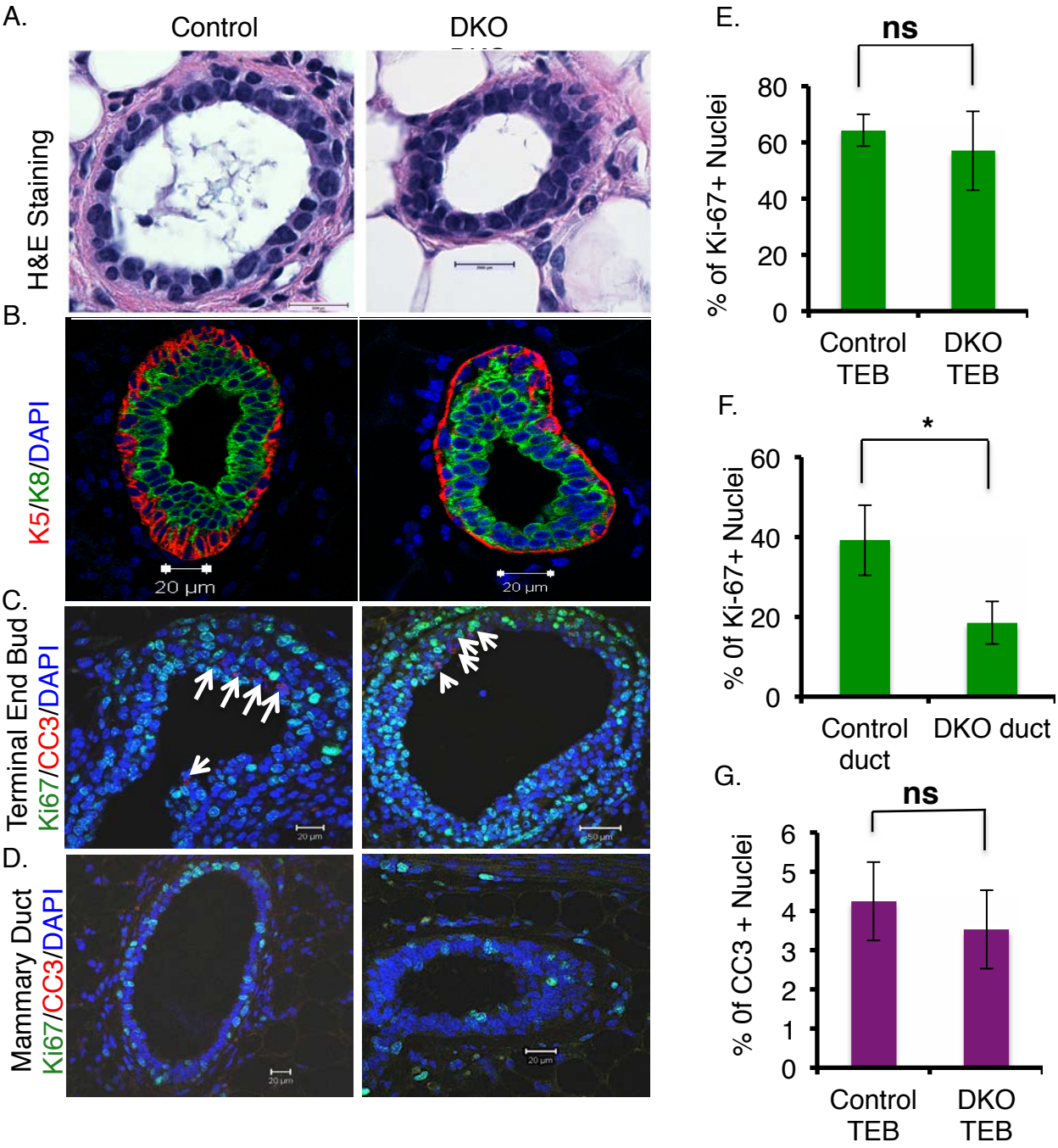

Figure S2. Histological and immuno-histological analyses of mammary gland to assess the impact of MMTV-Cre-mediated *Cbl/Cbl-b* DKO. (A) Hematoxylin and eosin (H&E) staining of formaldehyde-fixed and paraffin-embedded tissue sections of 6-week old *Cbl/Cbl-b* DKO and control mammary glands to show the lack of any obvious architectural defects in DKO mammary glands. (B) Immunofluorescence (IF) staining of *Cbl/Cbl-b* DKO and control mammary gland sections for basal (K5, red) and luminal (K8, green) cytokeratins. No differences in the luminal/basal organization are seen between DKO and control mammary glands. (C, D) Mammary gland sections from 6-week old control and DKO mice were stained with anti-Ki67 (green) and anti-cleaved caspase 3 (CC3, red) antibodies to visualize the proliferating and apoptotic cells within the terminal end buds and mammary ducts. Quantification was performed by scanning at least 15 high-power fields for proliferating (Ki67+) (E, F) and apoptotic (CC3+) (G) cells. Terminal end buds in control and DKO mammary glands show comparable levels of proliferation (E) and apoptosis (G). Mammary ducts in DKO mammary glands show a lower percentage of proliferating cells (F). Apoptotic events in mammary ducts were below the detection limit. Data shown are mean ± SEM, n=4 (independent sets). *, $p \leq 0.05$; ns, $p \geq 0.05$ (Student's t test).

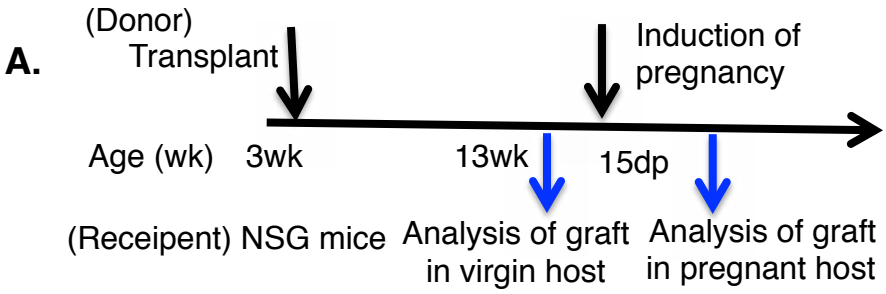

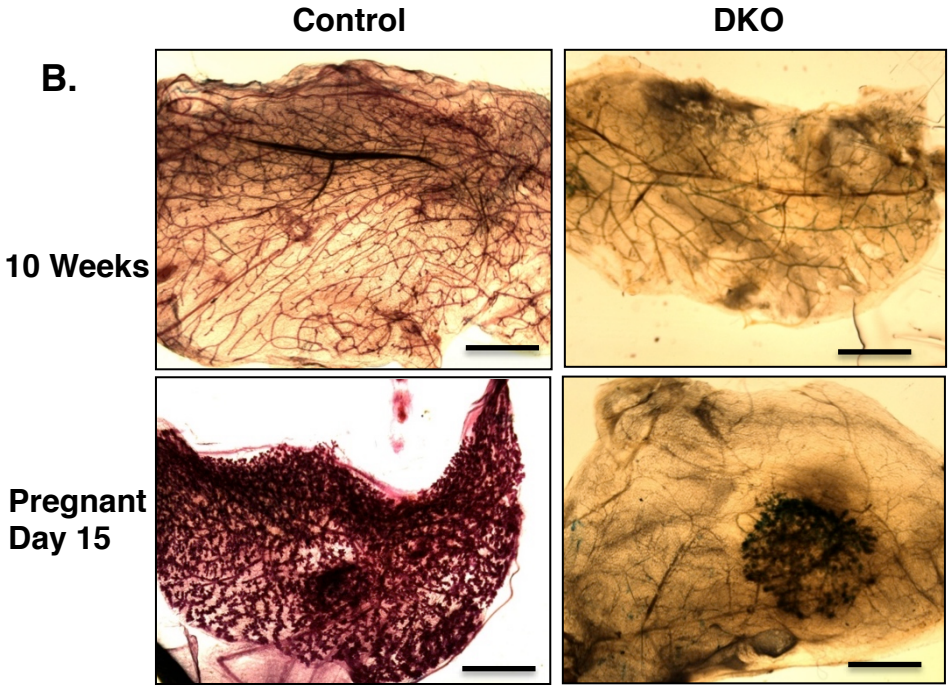

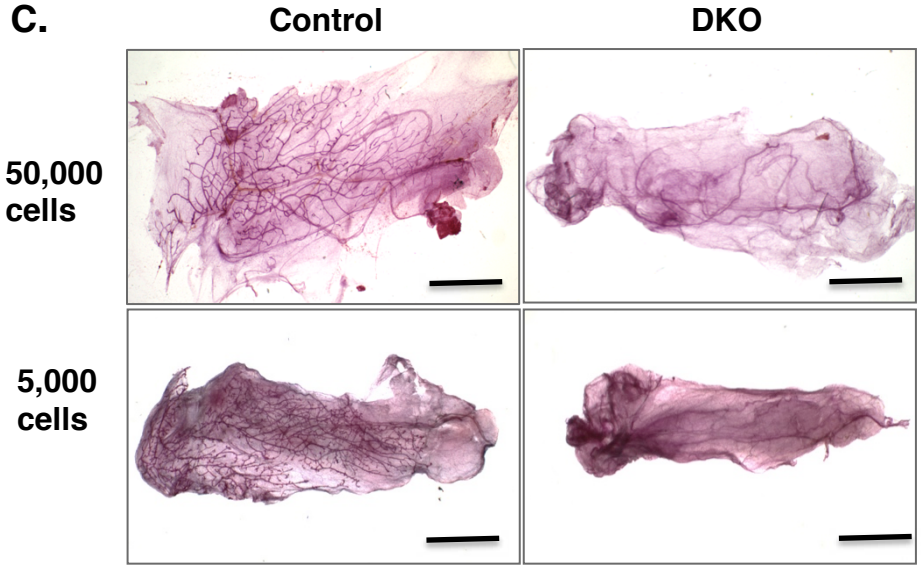

D.

Subsets	Genotype	# Cells	Take rate
Lin⁻ Unsorted	Control	50,000	5/5
	DKO	50,000	0/5
Lin⁻ EpCAM⁺	Control	5,000	4/7
	DKO	5,000	0/7

Figure S3. Reduced growth and branching of *Cbl/Cbl-b* DKO mammary glands upon transplantation, and defective mammary gland regenerating ability of isolated DKO mammary epithelial cells. (**A**) Schematic showing the time-line of tissue transplants and their analysis**.** (**B**) Mammary tissue fragments from MMTV-Cre based *Cbl/Cbl-b* DKO and control mice were transplanted into cleared mammary fat pads of 3-week old NOD/SCID/Gamma chain-deficient (NSG) mice and analyzed after 10 weeks**.** Each host received DKO and control transplants on the opposite sides. Whole-mount Carmine staining was carried out to visualize the growth and branching of glands formed from the transplanted mammary fragments. Less ductal elongation and branching is seen in DKO compared to control transplant. In transplant recipients analyzed at day 15 of pregnancy), transplanted DKO mammary fragments show a severe defect in ductal elongation compared to control although alveologenesis appears intact. Scale bar is 1 mm. (**C**) Lineage-negative mammary epithelial cells or $EpCAM^{+}$ epithelial cells from DKO or control mice were injected into cleared mammary fat pads on opposite sides of 3-week old NSG mice. Whole mounts of transplanted mammary fat pads were analyzed after 8 weeks to assess the ductal outgrowth. (**D**) Relative success of generating mammary outgrowths from transplanted mammary epithelial cells from control vs. DKO mice. Numbers in the last column indicate those positive for outgrowths vs. the total number transplanted (Take rate).

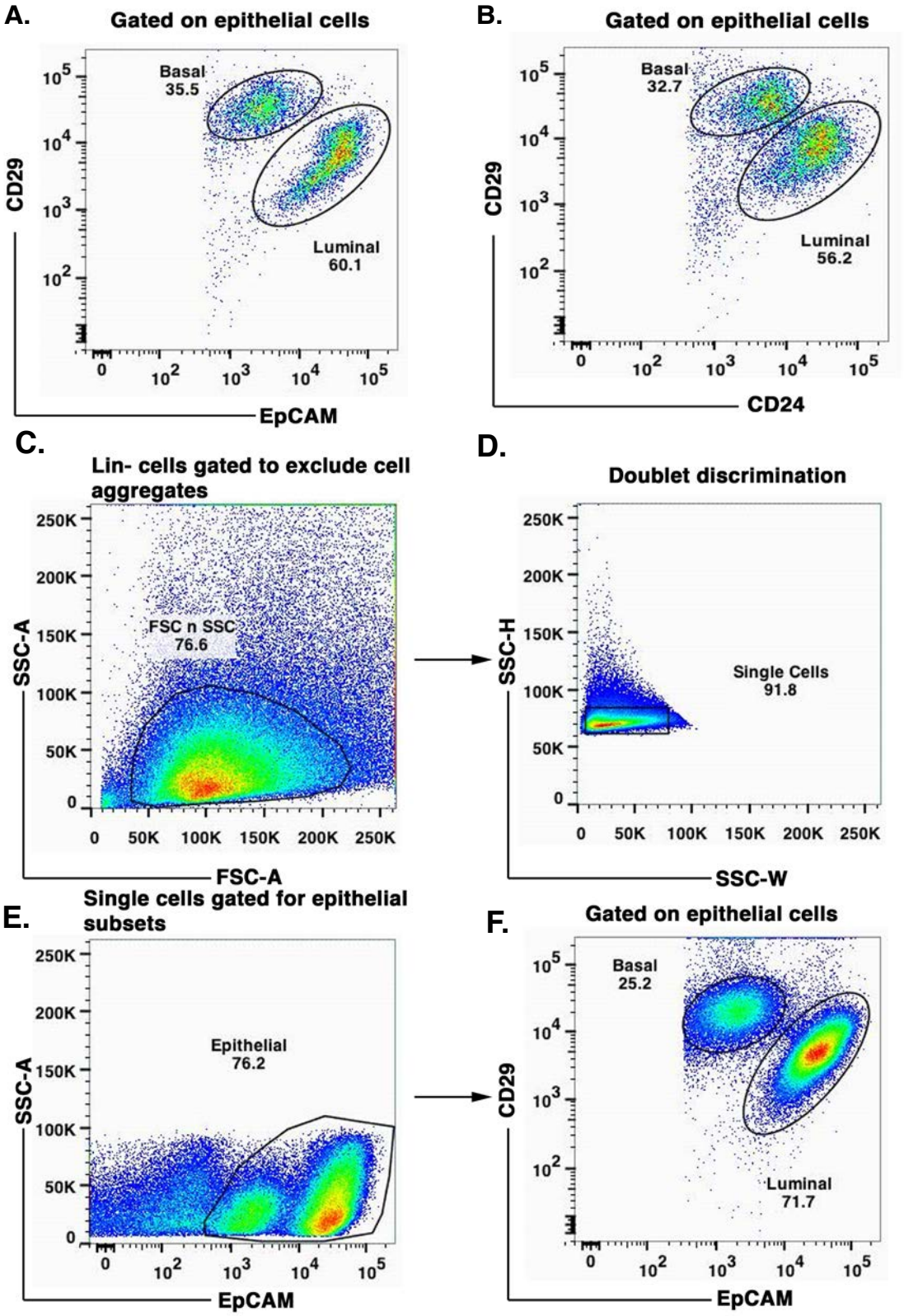

Figure S4. Typical plots of FACS-based separation of basal and luminal mammary epithelial cell populations using CD24 and EpCAM surface markers and the gating scheme used. Live Lin-negative (Lin-) cells were stained with fluorophore-labeled antibodies against mammary stem cell surface markers CD29, EpCAM or CD24. FACS plots showing the distribution of mammary epithelial cell populations from the same donor mouse when double-stained for CD24 and CD29 (A) or CD29 and EpCAM (B) marker combinations display comparable luminal and basal epithelial cell profiles, but better separation of the two fractions using CD29 and EpCAM combination. The flow cytometry gates based on forward (FSC) and side scatter (SSC) were used for exclusion of cell aggregates and dead cells (C), and to discriminate cell doublets from dual staining of single cells. (D). Gates used to demarcate the epithelial from stromal cells in double-staining analyses (E) and further separation of basal and luminal populations (F) are shown.

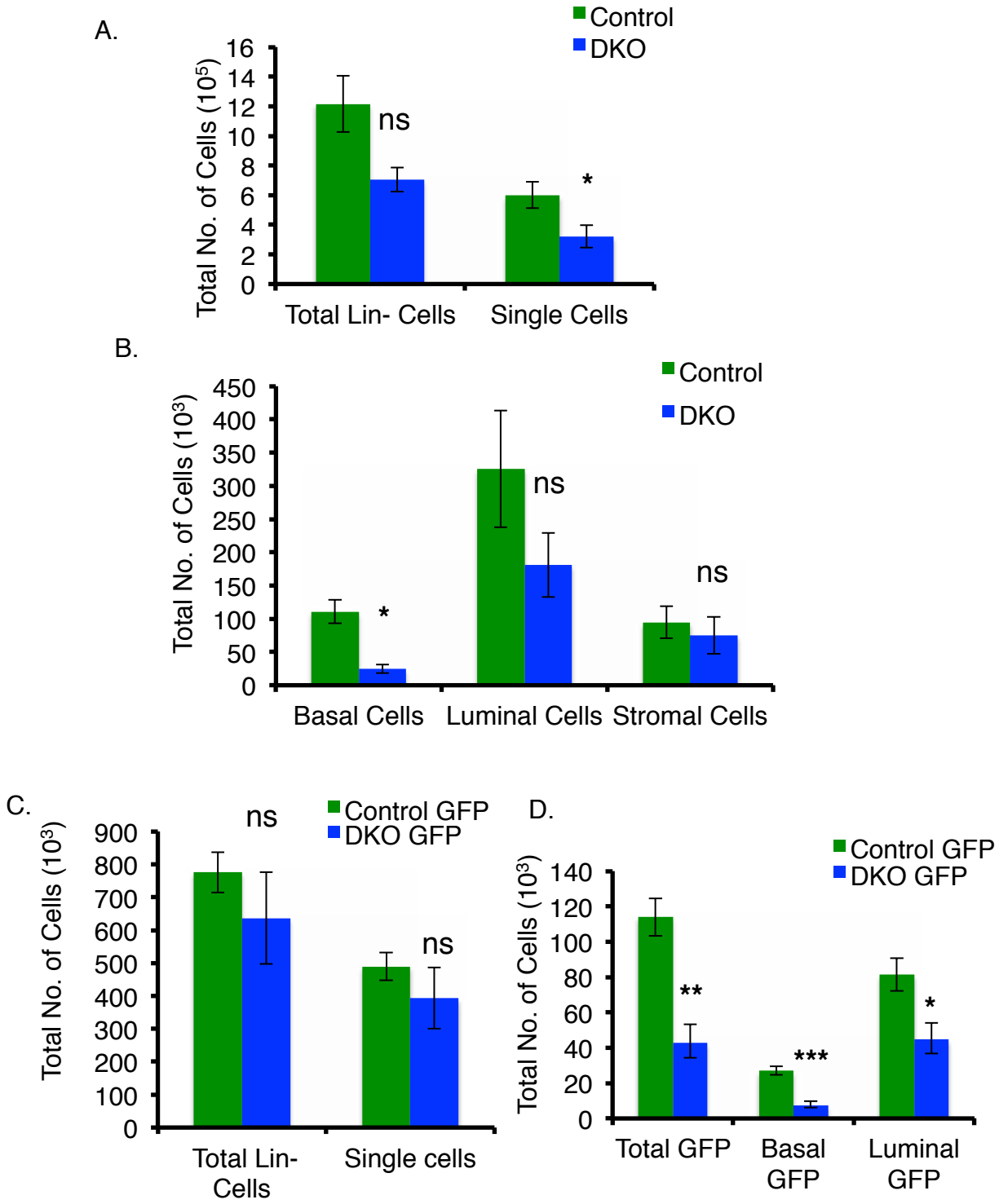

Figure S5. Reduction in the number of total mammary epithelial cells in MMTV-Cre-based *Cbl/Cbl-b* DKO mice as assessed by FACS analysis. (A-B) Lineage-negative mammary epithelial populations isolated from mammary glands of control or *Cbl/Cbl-b* DKO mice were gated for single cells by excluding doublets and dying cells as in Fig. S3 (A), and further gated to quantify the basal, luminal, and stromal populations (B). These analyses (n=6) show reduced yield of total Lin- single cells (A) and a selective reduction in the basal mammary epithelial cell pool in *Cbl/Cbl-b* DKO vs. the control mice. (C-D) Control or *Cbl/Cbl-b* DKO mice carrying a GFP reporter that is expressed after MMTV-Cre-mediated recombination were analyzed as in A-B. While differences in the numbers of total Lin- cells and single cells were not significant (C), the reduction in the numbers of GFP+ total single cells, basal cells and luminal cells was significant.

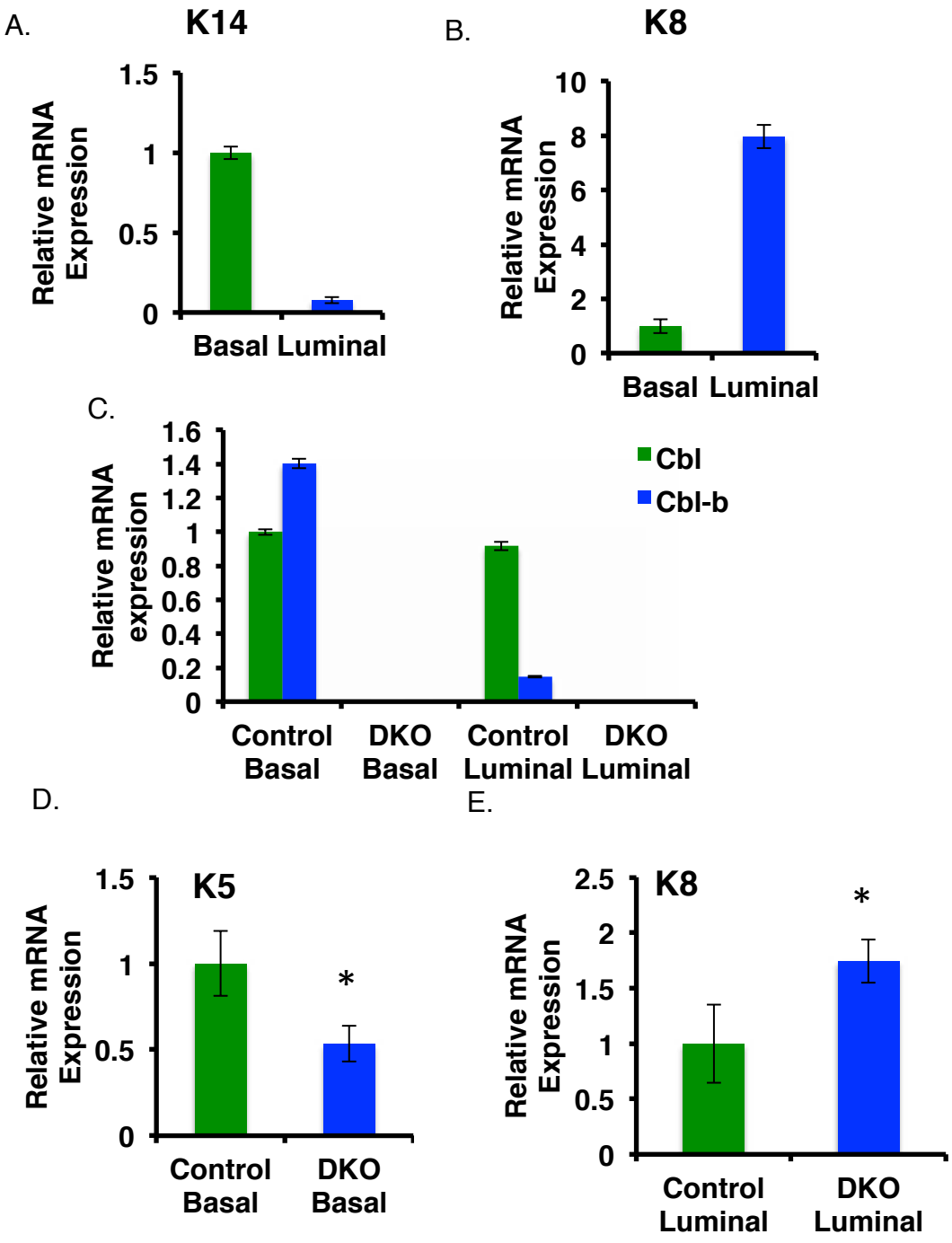

Figure S6. Demonstration of the lack of CBL and CBL-B expression in isolated mammary epithelial subsets. (A) The GFP+ cells within the basal and luminal subpopulations of isolated single mammary epithelial cell (as in Fig. S4C-D) were FACS-sorted based on CD29/EpCAM staining, and used to isolate RNA. The purity of sorted cells was analyzed by qPCR using primer sets specific to basal cytokeratin *K14* (A) or luminal cytokeratin *K8* (B), respectively. The basal population is enriched for cytokeratin *K14* while luminal cells are enriched for cytokeratin *K8*. (C) qPCR analysis was performed to quantify *Cbl* and *Cbl-b* mRNA expression relative to *GAPDH* as an internal reference control. Note the higher *Cbl-b* expression in the control basal compared to luminal population. Expression of both *Cbl* and *Cbl-b* is absent in DKO cell subsets. Concurrent qPCR analysis revealed reduced basal cytokeratin *K5* (D) and increased luminal cytokeratin *K8* (E) expression in DKO compared to control mammary cell subsets. Data shown are mean +/- SEM (n=3). ns, $p \geq 0.05$; *, $p \leq 0.05$, **, $p \leq 0.01$, ***, $p \leq 0.001$ by Student's t test.

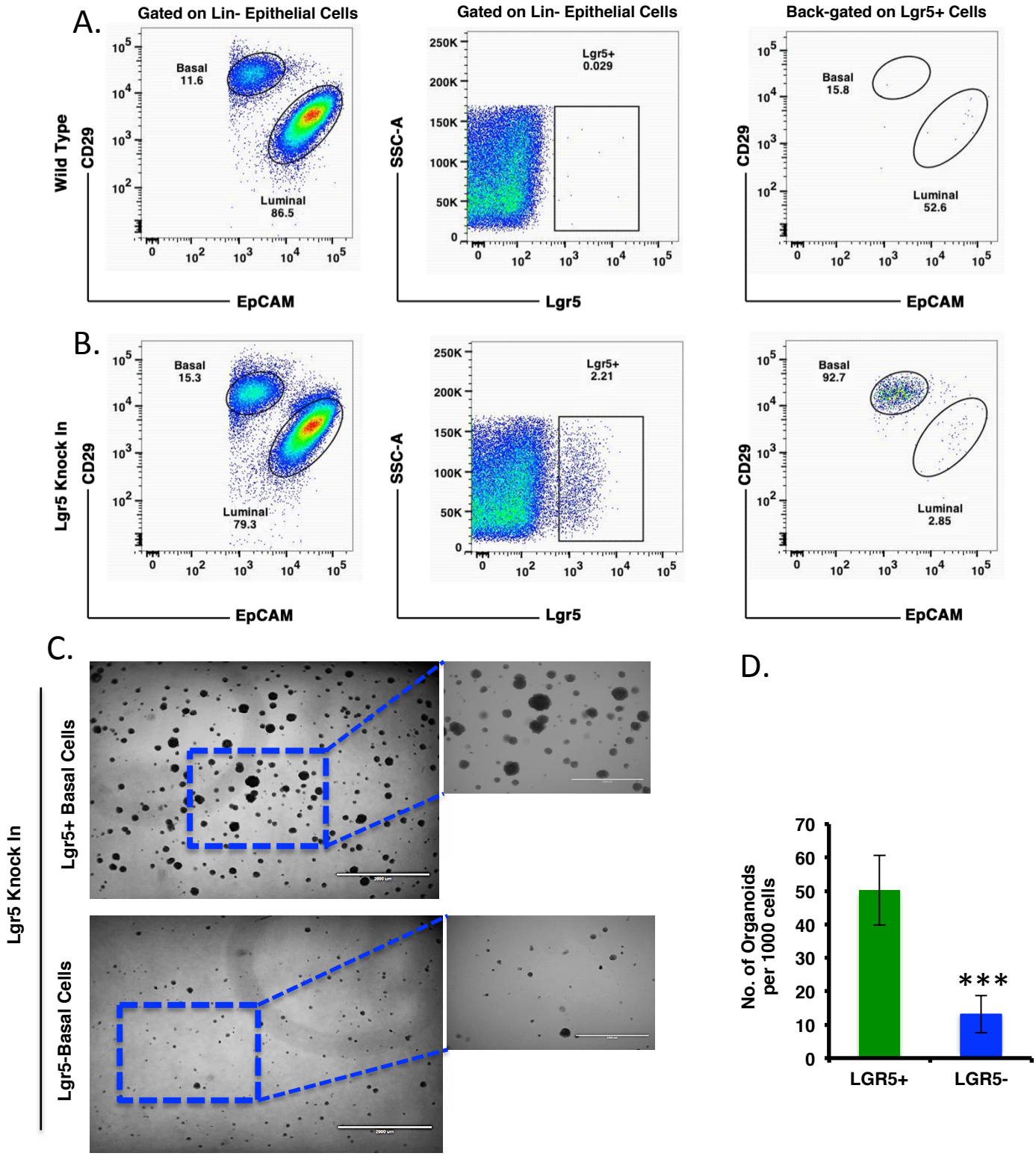

Figure S7. Compartmentalization of Lgr5+ mammary epithelial cells within the basal population, and validation of their self-renewal using the in vitro organoid-forming assay. Lineage-negative cells isolated from 5-week old WT (A) or Lgr5-GFP-IRES-CRE-ERT2 knock-in (Lgr5-GFP-Cre) (B) mice were analyzed by FACS for CD29, EpCAM and GFP. GFP+ cells (representing Lgr5+ cells) comprised 1-3% of epithelial cells; such cells were absent in WT MECs (upper panel), establishing the specificity of FACS-based analysis. Back-gating onto CD29/EpCAM-based subsets shows the majority of GFP+ cells to be within the basal cell compartment. The rare WT control cells seen within the GFP gate (<0.1%) did not specifically compartmentalize within the basal population. (C) The Lgr5+ (GFP+) and Lgr5- (GFP-) basal cells were isolated from Lgr5-GFP-IRES-CRE-ERT2 knock-in (Lgr5-GFP-Cre) mice, and analyzed in the organoid-forming assay. (D). Quantification of the organoid-forming assay data, shown as mean +/- SEM (n=3). ns, $p \geq 0.05$; *, $p \leq 0.05$; **, $p \leq 0.01$; ***, $p \leq 0.001$, by Student's t test. Majority of organoid-forming ability resides in the Lgr5+ basal cell fraction.

A.

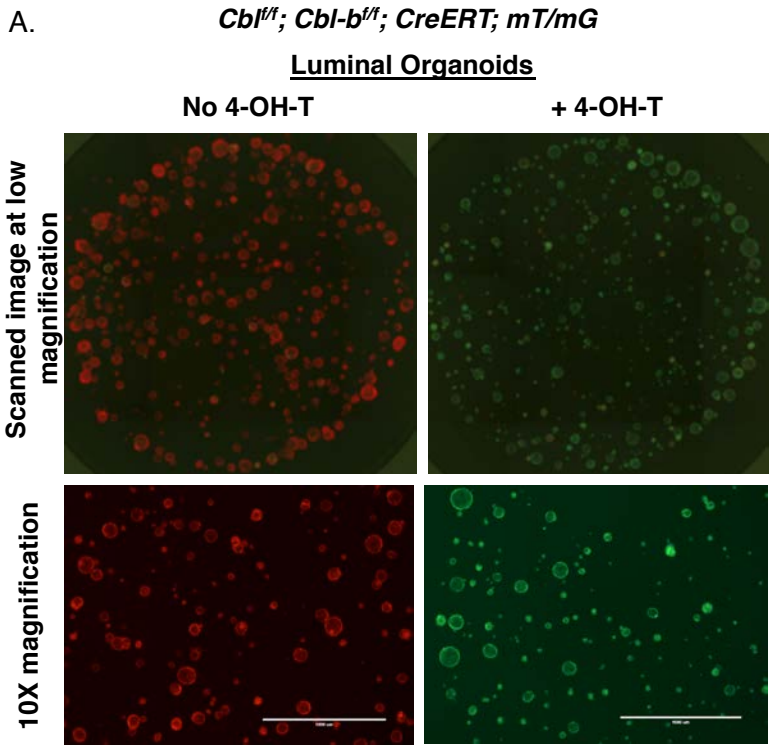

B.

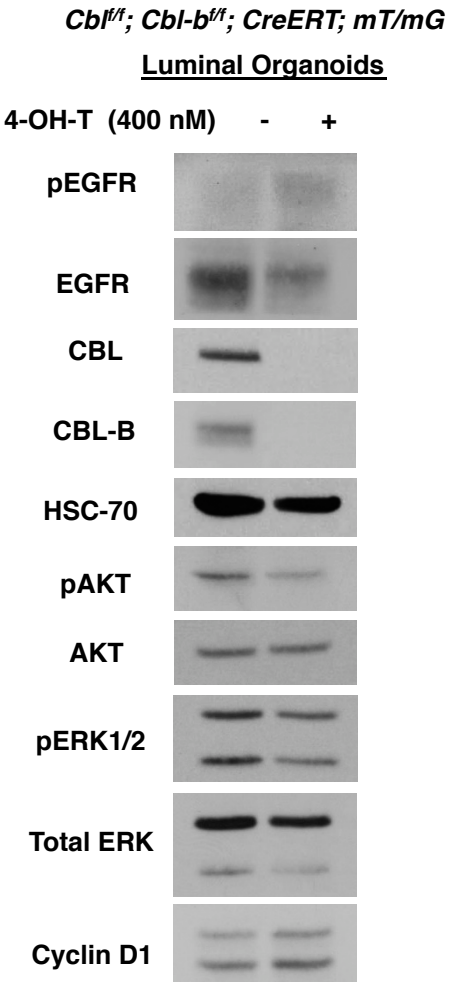

C.

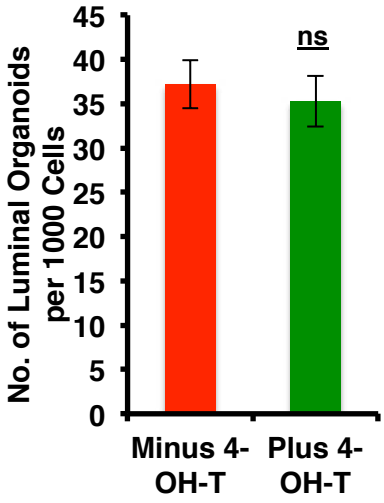

Figure S8. Luminal organoid-forming efficiency is unaltered upon tamoxifen-induced, CreERT-mediated, in vitro deletion in a model of *Cbl/Cbl-b* double-floxed model. (**A**) Luminal mammary epithelial cells isolated from 8 week-old *Cbl$^{f/f}$; Cbl-b$^{f/f}$; CreERT; mT/mG* (conditional DKO) were established in organoid cultures and treated with or without 4-OH-T to induce *Cbl/Cbl-b* deletion, as in earlier figures; the gene deletion is tracked using the dual fluorescent reporter). The non-induced or 4-OH-T-induced primary organoids formed by isolated luminal cells from *Cbl$^{f/f}$; Cbl-b$^{f/f}$; CreERT; mT/mG* (conditional DKO) to assess the self-renewal ability. Loss of red (RFP) and gain of green (GFP) fluorescence indicates successful CreERT activation and *Cbl/Cbl-b* deletion, which was confirmed by blotting, (B). (C) Quantitation of organoid numbers from (A). Data are shown as mean +/- SEM**.** n=3; ns, p≥0.05, *, p≤ 0.05, **, p≤0.01, ***, p≤0.001 by *Student's t* test.

Table S1. Nomenclature of mouse strains and their genotypes as used in this study.

Designation	**Genotype**
Control	$Cbl^{f/+}$; Cbl-$b^{+/-}$; MMTV-Cre(0/0) or $Cbl^{f/f}$; Cbl-$b^{+/-}$; MMTV-Cre(0/0)
Cre Control	$Cbl^{f/+}$; Cbl-$b^{+/-}$; MMTV-Cre(Tg/0)
Cbl KO	$Cbl^{-/-}$
Cbl-b KO	$Cbl^{f/f}$; Cbl-$b^{-/-}$; MMTV-Cre(0/0)
DKO/LacZ	$Cbl^{f/f}$; Cbl-$b^{-/-}$; MMTV-Cre(Tg/0); R26R
DKO/GFP	$Cbl^{f/f}$; Cbl-$b^{-/-}$; MMTV-Cre(Tg/0); CAG-GFP
MaSC- DKO	$Cbl^{f/f}$; $Cbl^{-/-}$; Lgr5-eGFP-IRES-CRE-ERT; R26R
MaSC-Control	$Cbl^{f/+}$; $Cbl^{+/-}$; Lgr5-eGFP-IRES-CRE-ERT; R26R or Lgr5-eGFP-IRES-CRE-ERT
Conditional DKO	$Cbl^{f/f}$; $Cbl^{f/f}$; CreERT; mT/mG

Table S2. List of primers used for PCR-based genotyping of various alleles.

Gene Allele	**Forward 5'-3'**	**Reverse 5'-3'**
Cbl WT	AAGTTCCAAGCCTAGCCAGATAT GTGTGTG	TCCCCTCCCCTTCCCATGTTTT TAATAGACTC
Cbl del	TGGCTGGACGTAAACTCCTCTTCA GACCAATAAC	TCCCCTCCCCTTCCCATGTTTT TAATAGACTC
Cbl floxed	GTGGTGGCTTGCAATTATAATCCT ACCACTTAGG	GTTTGAGATGTCTGGCTGTGTACAC GCG
Cbl-b del	CCCAGCAAAAGTAGCCAATG	CTTGCAAAAAGGACTAAGATTC
Cbl-b floxed	GGCAGAACCACTGAGACACATTT A	GGCTGCCAAACTGCTACCCAGGAG
MMTV-Cre	GCGGTCTGGCAGTAAAAACTATC	GTGAAACAGCATTGCTGTCACTT
Lgr5-eGFP-IRES-CRE-ERT (WT)	CTGCTCTCTGCTCCCAGTCT	ATACCCCATCCCTTT TGAGC
Lgr5-eGFP-IRES-CRE-ERT (Mutant)	CTGCTCTCTGCTCCCAGTCT	GAACTTCAGGGTCAGCTTGC
R26R-LacZ	AATCCATCTTGTTCAATGGCCGAT C	CCGGATTGATGGTAGTGGTC
CAG-GFP	GCACTT GCTCTCCCAAAGTC	GTTATGTAACGCGGA ACT CC
Rosa 26 –mT/ mGFP	CTCTGCTGCCTCCTGGCTTCT	TCAATGGGCGGGGGTCGTT

Table S3. List of real time PCR primers used to detect mRNA levels of the indicated genes.

Target	**Forward 5'-3'**	**Reverse 5'-3'**
Cbl	AGCTGATGCTGCCGAATTT	TTGCAGGTCAGATCAATAGTGG
Cbl-b	GGAGCTTTTTGCACGGACTA	TGCATCCTGAATAGCATCAA
Cbl-c	GCCACCTGCCTGCCTTTGAC	GCTACTTGGAGAGGTGGCAAAG
K14	TGAGAGCCTCAAGGAGGAGC	TCTCCACATTGACGTCTCCAC
K5	GAGATCGCCACCTACAGGAA	TCCTCCGTAGCCAGAAGAGA
K8	AGATCACCACCTACCGCAAG	TGAAGCCAGGGCTAGTGAGT
GAPDH	CCTGGAGAAACCTGCCAAGTATG	AGAGTGGGAGTTGCTGTTGAAGT